REMARKS

The specification was amended to correct the informalities regarding the units of measure that were objected to by the examiner. Claims 1-2, 8, 13, 18-21, 28-33, 35, 40, 43, and 45 have been amended and claims 3, 9, 36-39, and 46 have been canceled. Claims 1-2, 4-8, 10-35, and 40-45 are pending in this application.

In the Office Action of June 21, 2005, the drawings were objected to under 37 C.F.R. § 1.83(a) for not including a stinger pipe as claimed in claim 9. Claim 9 was canceled, so the drawings do not require amendment.

Claims 1, 13, 19-21, 28, 29, 31, and 38 were objected to because of various informalities. Claim 1 was amended such that the subparts of the claim begin with lowercase letters and the word "and" was added between the final subpart and the subpart preceding the final subpart. Claims 13, 19, 20-21, 29, and 31 were amended to change the words "further comprising" to "wherein". Claim 28 was amended to conform the units of measure to the proper form. These amendments were made to remove informalities, not to address any issues directed to the merits of the patentability of the subject matter of the invention.

Claims 1-46 were rejected under 35 U.S.C. § 112 as being indefinite for failing to particularly point out and distinctly claim the subject matter which applicant regards as the invention. Claims 1-2, 8, 18-21, 29-30, 32-33, 35, 40, 43, and 45 were amended and claims 3, 9, 36-39, and 46 were canceled. Applicants respectfully traverse this rejection based on the claims as currently amended.

Claim 1 was amended to "a combination" instead of "the combination" since there was no antecedent basis for using "the". Claims 2 and 43 were amended to clarify the structural limitation being recited in the claims. Claim 3 was canceled in response to the examiner's rejection. Claim 8 was amended to clarify the structural limitation recited by the claim and to remove the ambiguity relative to "a support" and "a/said support" as set forth in claims 6 and 7. Claim 9 was canceled in response to the examiner's rejection. Claim 18 was amended to remove the trademark/trade names of Hastelloy and Inconel. Claim 19 was amended to clarify the structural limitation recited by the claim that the membrane support is located between the membrane and the catalyst. Claim 20 was amended to clarify the structural limitation recited by the claim. Claim 21 was amended

to remove the structural limitation that was the subject of the examiner's rejection. Claims 29 and 30 were amended to clarify the structural limitation recited by the claims. Claims 32 and 33 were amended to be more specific concerning the meaning of high pressure. Claim 35 was amended to remove the term considered vague and indefinite by the examiner. Claims 36-39 were canceled in response to the examiner's rejection. Claim 45 was amended to clarify the structural limitation recited by the claim and to correct the antecedent basis. Claim 46 was canceled in response to the examiner's rejection.

Claims 1-8, 10-15, 17, 19-21, 25, 29, 30, 36-43 and 45 were rejected under 35 U.S.C. § 103(a) as being unpatentable over Minet et al. (U.S. 5,229,102) in view of Mikus et al. (WO 99/18392). Applicants respectfully traverse this rejection based on the claims as currently amended.

Minet et al. discloses an apparatus for steam reforming of a hydrocarbon to produce H_2, CO and CO_2 that uses a ceramic membrane to separate the hydrogen from the other streams. Mikus et al. discloses a flameless combustor process heater that has an oxidation reaction chamber with an inlet for oxidant and outlet for combustion products and a fuel conduit capable of transporting a fuel mixture to a plurality of fuel nozzles within the oxidation reaction chamber. The temperature of the combined mixture of oxidant and fuel is greater than the autoignition temperature of the combined mixture resulting in flameless combustion.

There is no suggestion to combine these two processes to produce the apparatus of the present invention, because Mikus et al. teaches that the use of a flameless combustor process heater in a steam reformer results in higher average temperatures. (Mikus et al., p. 17 lines 24-25). The membranes of the present invention do not operate well under the higher temperatures provided by the flameless combustor process heater in a steam reforming reactor as disclosed by Mikus et al., so it would not have been obvious for one of ordinary skill in the art to combine these two references to obtain the present invention.

There are two reasons that the membranes do not function effectively under the higher temperatures taught by Mikus et al. First, the membranes comprising palladium, platinum, nickel, silver, yttrium, cerium, holmium, lanthanum, gold and alloys thereof

undergo intermetallic diffusion at higher temperatures that results in decreased permeability, and second, the membranes comprising tantalum, vanadium, and niobium experience lower permeability at higher temperatures.

The membranes comprising metals from the first group that includes palladium, platinum, nickel, silver, yttrium, cerium, holmium, lanthanum, and gold cannot function at the higher average temperatures between "800 °C and 870 °C" as disclosed in Mikus et al. (p. 17, lines 12-13) because of the intermetallic diffusion that occurs. For example, the present application discloses that the maximum operating temperature of the palladium membranes is 550 °C. (p. 28, lines 18-19). In addition, Exhibit A to this response provides more clarification on the decreased permeability of the membranes at temperatures greater than 550 °C. This article, published in Vol. 44, No. 2 of the AIChE Journal, shows the drop in hydrogen flux across palladium membranes and provides graphs showing the deterioration in the hydrogen permeation rate at temperatures greater than 550 °C. (p. 318). The determination of the temperature at which intermetallic diffusion occurs is based on the Tamman temperature of the metal as discussed in Exhibit A. The range of Tamman temperatures of the first group of metals shows that membranes comprising these metals will experience intermetallic diffusion at temperatures less than the temperatures provided by the flameless combustor process heater as taught by Mikus et al., and thus it would not have been obvious for a person of ordinary skill to substitute the flameless combustor process heater as taught by Mikus et al. for the heater used in the steam reforming reactor disclosed by Minet et al.

Tamman temperatures are calculated based on the melting points of each metal, and these melting points were obtained from the CRC Handbook of Chemistry and Physics, 71st Edition. Palladium has a melting point of 1554 °C and a Tamman temperature of 640 °C; platinum has a melting point of 1772 °C and a Tamman temperature of 750 °C; nickel has a melting point of 1453 °C and a Tamman temperature of 590 °C; silver has a melting point of 962 °C and a Tamman temperature of 345 °C; yttrium has a melting point of 1522 °C and a Tamman temperature of 625 °C; cerium has a melting point of 798 °C and a Tamman temperature of 263 °C; holmium has a melting point of 1470 °C and a Tamman temperature of 599 °C; lanthanum has a melting point of 918 °C and a Tamman temperature of 323 °C; and gold has a melting point of 1064 °C

and a Tamman temperature of 396 °C. These melting points and Tamman temperatures were rounded to the nearest degree.

Tantalum, vanadium and niobium do not have low Tamman temperatures, but the decreased permeability to hydrogen of membranes comprising tantalum, vanadium and niobium at higher temperatures is shown in an article titled Hydrogen Transport through Tubular Membranes of Palladium-Coated Tantalum and Niobium, attached here as Exhibit B. Figure 1 of Exhibit B shows the increased hydrogen permeability for tantalum, vanadium and niobium at lower temperatures. Due to this relationship between the temperature and the hydrogen permeability, it would not have been obvious for one of ordinary skill in the art to utilize the flameless combustor process heater of Mikus et al. disclosed as useful for providing higher reaction temperatures, in a steam reforming reactor as disclosed in Minet et al. Therefore, the present invention would not have been obvious to one of ordinary skill in the art based on the prior art of Minet et al. and Mikus et al.

Claim 9 was rejected under 35 U.S.C. §103(a) as being unpatentable over Minet et al. in view of Mikus et al., as applied to claim 1, and further in view of Shirasaki et al. (US 5,639,431). Claim 9 has been cancelled.

Claims 16, 18, 22 and 25-28 were rejected under 35 U.S.C. §103(a) as being unpatentable over Minet et al. in view of Mikus et al., as applied to claim 1, 12 and 13, and further in view of Lin et al. (EP 1 024 111). Applicants respectfully traverse this rejection. Claims 16, 18, 22 and 25-28 are all dependent on claim 1, and are not obvious for the reasons discussed with respect to claim 1 above.

Claim 23 was rejected under 35 U.S.C. §103(a) as being unpatentable over Minet et al. in view of Mikus et al. and Lin et al., as applied to claims 1, 12 and 22, and further in view of Juda et al. (US 5,904,754) or Rosset (US 2,958,391) or Behr et al. (US 4,496,373). Applicants respectfully traverse this rejection. Claim 23 is dependent on claim 1, and is not obvious for the reasons discussed with respect to claim 1 above.

Claim 24 was rejected under 35 U.S.C. §103(a) as being unpatentable over Minet et al. in view of Mikus et al. as applied to claims 1 and 12, and further in view of Rosset. Applicants respectfully traverse this rejection. Claim 24 is dependent on claim 1, and is not obvious for the reasons discussed with respect to claim 1 above.

Claims 31-35 and 46 were rejected under 35 U.S.C. §103(a) as being unpatentable over Minet et al. in view of Mikus et al as applied to claim 1, and further in view of Topsoe (US 5,169,717). Applicants respectfully traverse this rejection. Claims 31-35 are all dependent on claim 1, and are not obvious for the reasons discussed with respect to claim 1 above. Claim 46 has been canceled.

In light of the above, Applicants respectfully request allowance of the pending claims in the application.

Respectfully Submitted,

WELLINGTON, Scott Lee et al.

By their attorney : _____

Richard B. Taylor
Reg. No. 37,248
Shell Oil Company
(713) 241-3558

Exhibit A

Duplicate

Defect-Free Palladium Membranes on Porous Stainless-Steel Support

Peter P. Mardilovich, Ying She, and Yi Hua Ma
Dept. of Chemical Engineering, Worcester Polytechnic Institute, Worcester, MA 01609

Min-Hon Rei
China Technical Consulting, Inc., Taipei, Taiwan, R.O.C.

Defect-free Pd membranes were prepared by an electroless plating technique on porous stainless-steel tubes. The effective surface of Pd membranes was up to 75 cm^2. The helium flux was not detected at room temperature and pressure difference of 3 atm. At 350°C hydrogen permeances of up to 8 $m^3/(m^2 \cdot h \cdot atm^{0.5})$ were obtained. At a pressure difference of 1 atm and 350°C, selectivity coefficients as high as $J(H_2/J(N_2) = 5{,}000$ were observed. Fluxes of gases, impermeable through the Pd, were quantitatively described as a combination of Knudsen diffusion and viscous flow through the gaps created in the Pd layer at high temperatures. The stability of the prepared membranes at temperatures up to 700°C was investigated. The membranes were stable at 350°C over a period of 1,100 h, with no significant changes in the steady-state hydrogen flux and with a recrystallization texture and aggregation of Pd grains.

Introduction

The development of high-temperature processes and tighter environmental regulations requires utilization of gas separation processes that will provide high fluxes, high selectivity of separation, and the ability to operate at elevated temperatures. Hydrogen separation and purification from a reaction gas mixture is an area of particular interest in this respect. Dense metal membranes are especially well suited for high-temperature hydrogen separations. Palladium and its alloys are the most commonly used materials for the preparation of dense metal membranes because of their high hydrogen permeability and chemical resistance (McBride and McKinley, 1965). Compared with unsupported metal membranes, the development of an asymmetric composite membrane with a porous support and thin Pd or Pd-alloy dense layer would provide both higher transmembrane flux and lower Pd loading in the membrane.

There are several major techniques for the deposition of Pd or its alloys on a support. A spray pyrolysis method was used by Li et al. (1993) to deposit a Pd-Ag alloy on the alumina support. Yan et al. (1994) and Morooka et al. (1995) formed a thin palladium membrane inside the porous wall of an α-alumina support tube by the metal-organic chemical-vapor deposition (MOCVD) technique by decomposing palladium (II) acetate in argon under reduced pressure. A thin (1–2 μm) Pd layer was also pyrolytically deposited by the supercritical fluid transport-chemical deposition (SFTCD) method using the metal β-diketonate complex—(2,2,7-trimethyl-3,5-octanedionato) palladium (II) (Hybertson et al., 1991). Ultrathin Pd composite membranes were prepared by the sputter-deposition technique on polymeric membranes (Athayde et al., 1994), porous alumina (Jayaraman et al., 1995a,b), anodic alumina (Konno et al., 1988; Mardilovich et al., 1996a), and Vycor glass (Bryden and Ying, 1995) supports. Gryaznov et al. (1993) prepared Pd and Pd-alloy membranes on polymer membranes, porous stainless steel, and oxide plates by magnetic sputtering. Recently (Peachey et al., 1996), electron-beam evaporation and ion-beam sputtering were used to deposit Pd on the surface of tantalum foil. Some other examples of the application of these techniques, as well as physical vapor deposition and electroplating, were briefly discussed in the review by Shu et al. (1991). The major drawbacks of all these powerful techniques, especially useful for the deposition of alloys, are the low area of the prepared membranes and/or high cost of the necessary equipment. The practical applicability of these techniques may require further investigation.

Correspondence concerning this article should be addressed to Y. H. Ma.

On the other hand, electroless plating appears to be quite attractive due to the possibility of uniform deposition on complex shapes and large substrate areas, hardness of the deposited film, and very simple equipment. Electroless plating has been used to produce Pd or Pd-alloy membranes on a wide variety of supports, which include tantalum and niobium tubes (Buxbaum and Marker, 1993; Buxbaum and Kinney, 1996), porous silver (Govind and Atnoor, 1991), porous glass (Uemiya et al., 1988, 1991a), alumina (Uemiya et al., 1991b; Kikuchi and Uemiya, 1991; Collins and Way, 1993), and porous stainless steel (Shu et al., 1993; Mardilovich et al., 1996b; Yeung et al., 1996). Recently, Yeung and Varma (1995) proposed a method of preparation of Pd-composite membranes by using osmotic pressure for the manipulation of the microstructure, porosity, and thickness of the deposited metal.

The main advantages of porous stainless-steel (PSS) supports over porous ceramics, Vycor glass, Ta, V, and so forth, are the resistance to cracking and the simplicity of module construction. Composite Pd/PSS membranes, welded from both ends with nonporous stainless-steel tubes, can be very easily assembled. Additionally, the thermal expansion coefficient of stainless steel is almost identical to that of palladium, ensuring good mechanical properties of the composite membrane during temperature cycling. The first attempt to use PSS as the support was reported by Shu et al. (1993), using a disk with the geometric area of 2 cm^2, but permeation data were not reported. Data presented by Yeung et al. (1996) indicated that palladium-PSS composite membranes could give high hydrogen fluxes and selectivities. Their results appear to show that the synthesis procedure based on electroless plating with osmosis gives membranes with higher fluxes and better thermal stability than the conventional electroless plating.

The objective of this study is to investigate factors affecting the preparation of dense, defect-free palladium membranes on porous stainless-steel supports and to study the transport mechanisms through the prepared membranes.

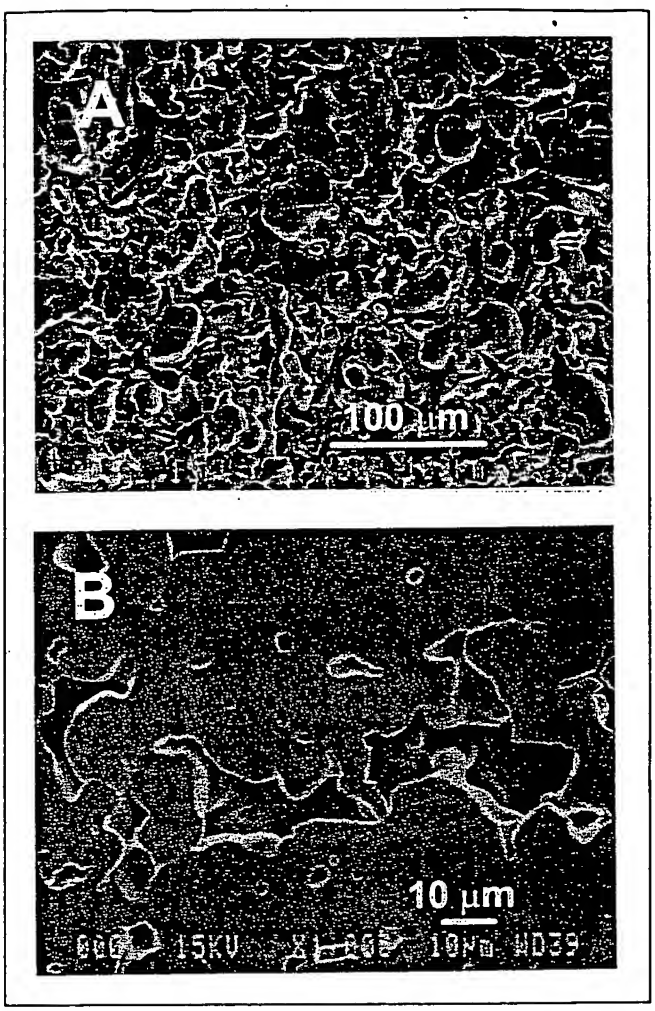

Figure 1. Scanning electron micrographs: (A) original; (B) polished grade 0.5 porous stainless steel.

Experimental

Porous stainless-steel support

Porous 316L stainless-steel cups and tubes (OD—15.9 and 12.7 mm; wall thickness—1.6 mm; length—19 and 25 mm for cups and 152 mm for tubes) were purchased from Mott Metallurgical Corporation. According to the manufacturer, the grade of these PSS was 0.5 μm (95% rejection) with 5 μm the biggest pore diameter and an average pore diameter of 3 μm (Mott Metallurgical, 1995). The porosity of PSS was 17%. The PSS cups and tubes were electrically welded to nonporous stainless-steel tubes.

Figure 1 shows the SEM pictures of a typical grade 0.5-μm PSS. There are a number of holes on the surface with the dimension around 20–30 μm, as shown in Figure 1a. However, it appears that only the entrance of the pore has such a large size. Below the surface they rapidly became narrower and, in general, the diameter of the real pores does not exceed 8 μm, as can be seen from the SEM picture of the preliminary polished PSS sample, shown in Figure 1b. The presence of such large and deep holes can be an additional difficulty in the deposition of the dense palladium layer. On the other hand, these holes, or entrances into the pores, can improve adhesion strength between the Pd film and PSS surface, which depends on the mechanical bonding and the anchoring effects (Honma and Kanemitsu, 1987).

An important characteristic of plating palladium on the PSS is the strength of the bond that can develop between the base stainless steel and the palladium layer. Metal-to-metal bonds with high adhesion values require thorough surface preparation to present a clean and optimally rough surface structure. Foreign contaminants (grease, oil, dirt, corrosion products, and others) should be completely removed from the stainless-steel surface. This was achieved by mechanical treatment (sandpaper, stainless-steel brush, file, etc.) and cleaning the PSS in an ultrasonic bath with alkaline solution at ~ 60°C followed by rinsing in tap water, deionized water, and isopropanol. The alkaline cleaning solution consisted of a combination of alkaline sodium compounds such as hydroxide, carbonate, phosphate, and organic detergent.

The roughness of the stainless-steel surface was increased by a ~ 5 min treatment in concentrated hydrochloric acid, followed by water rinsing. Such a treatment also provided the

preactivation of the support surface. The rust on the surface caused by the hydrochloric acid treatment was removed by diluted (~ 40%) phosphoric acid.

Activation

The membranes went through a surface activation prior to the electroless plating. The purpose of the surface activation was to seed the PSS surface with palladium nuclei, which during the electroless plating initiated the autocatalytic process of reducing the metastable Pd salt complex on the target surface. The activation procedure consisted of successive immersions in an acidic $SnCl_2$ bath (sensitizing) followed by an acidic $PdCl_2$ bath. After immersion in the $SnCl_2$ bath, a gentle rinsing with deionized water was used. Rinsing with 0.01 M HCl and then with water was carried out after immersion in the $PdCl_2$ bath. The 0.01 M HCl solution was used to prevent hydrolysis of Pd^{2+} ions. The typical composition of the activation bath is presented in Table 1.

During rinsing with deionized water after immersion in the acidic $SnCl_2$ bath, the partial hydrolysis of Sn^{2+} took place to form little (poorly) soluble product, $Sn(OH)_{1.5}Cl_{0.5}$, and other more complicated hydroxy-chlorides (Melashchenko, 1987). Such tin hydroxy-chlorides were strongly attached to the surface as a layer with a thickness of a thousandth-tenth of a micron. The composition, structure, and thickness of this layer depended on the ratio $HCl/SnCl_2$, support surface structure, roughness and shape, and the hydrodynamic regime of rinsing.

An excess of Sn^{2+} on the target surface of porous stainless steel can create a loose (crumbly), easy-to-peel layer, while a deficiency of Sn^{2+} can lead to nonuniform seeding of the palladium nuclei. The distribution of catalytic centers for autocatalytic Pd^{2+} reduction must be dense and uniform at an optimum concentration of Sn^{2+} on the surface. To reach this goal, a two-step immersion sequence in $SnCl_2$ and $PdCl_2$ solutions was generally repeated 4–10 times, depending on the intensity of the activation. A perfectly activated layer has a uniform dark-brown color and smooth surface. If the quality of the activated layer was unsatisfactory, it was removed in an ultrasonic bath with 1-M HCl and the activation procedure was repeated.

After 10 sensitizing/activation cycles, followed by drying at 120°C for 2 h, the thickness of the activated layer was around 1.5 μm, as can be seen in Figure 2a. The density of the layer, which consisted mainly of $Sn(OH)_4$ and Pd nuclei, was around 3–3.5 g/cm^3. After 5 min treatment by 1-M HCl, the activated layer became fragile, and its porous structure is shown in Figure 2b.

The activation layer can be considered as a sandwich structure consisting of a number of very thin layers, one after each sensitizing/activation cycle, with Pd nuclei on the top of each layer. A thicker activated layer results in higher density of Pd nuclei on the support surface, but lowers the adhesion of further deposited Pd layers to the PSS support. In many cases, the optimum activated layer was created after six sensitizing/activation cycles.

Table 1. Composition of the Activation Solutions

	Sn Solution	Pd Solution
$SnCl_2 \cdot 2H_2O$, g/L	1.0	—
$PdCl_2$, g/L	—	0.1
HCl (~ 37%), ml/L	1	1
Temperature, °C	20°C	20°C
Duration, min	5	3–5

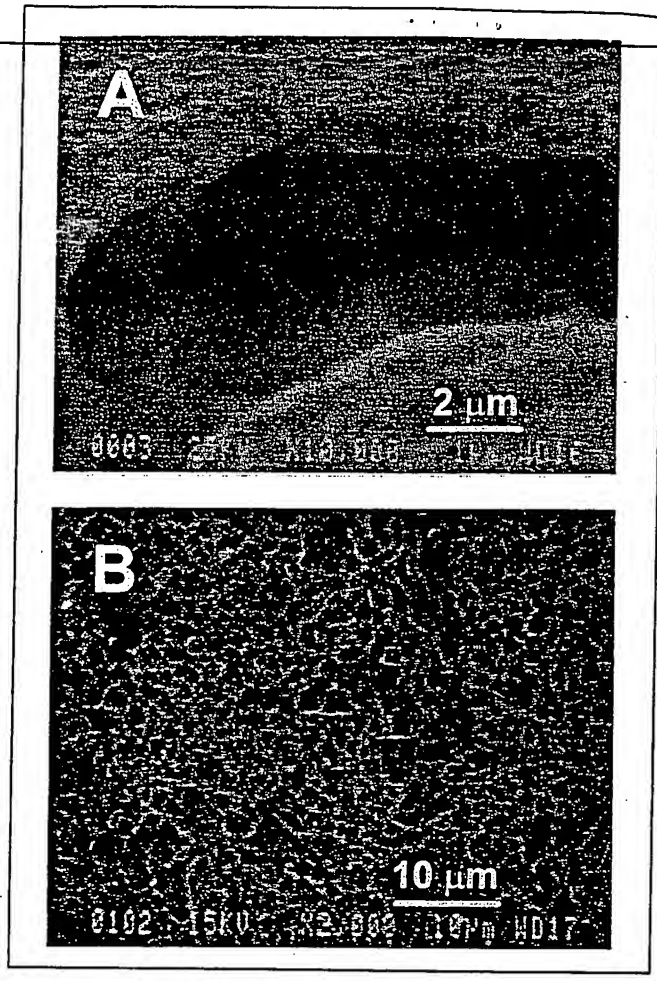

Figure 2. (A) Cross section of activated layer after 10 sensitizing/activation cycles; (B) top view of the partially removed activated layer.

Deposition of palladium

Palladium deposition occurs according to the following autocatalytic reaction

$$2Pd(NH_3)_4Cl_2 + H_2NNH_2 + 4NH_4OH \rightarrow 2Pd + N_2 + 8NH_3 + 4NH_4Cl + 4H_2O$$

or

$$2Pd^{2+} + H_2NNH_2 + 4OH^- \rightarrow 2Pd^0 + N_2 + 4H_2O.$$

Preseeded palladium nuclei at the activation stage reduce the induction period of the autocatalytic process at the beginning of the deposition.

Table 2. Composition of the Electroless Palladium–Plating Bath

$Pd(NH_3)_4Cl_2 \cdot H_2O$, g/L	4.0
NH_4OH (28%), mL/L	198
Na_2EDTA, g/L	40.1
H_2NNH_2 (1 M), mL/L	5.6–7.6
pH	~10.4
Temperature, °C	60
$V_{solution}/S_{plating\ area}$, cm^3/cm^2	~3.5

Table 2 shows a typical plating bath composition. Palladium was deposited on PSS cups by suspending the cups in an electroless-plating bath surrounded by a water jacket for temperature control. For the deposition of palladium on the long tube support a special electroless-plating cell was used. The bath used for the deposition on long tubes is presented in Figure 3. A uniform deposition of Pd on the PSS long tube was achieved by controlled rotation of the support.

The designed cell also allowed for the control of the rate of deposition. The flow of the gases evolved from this reaction was quantitatively measured by a soap-bubble flowmeter. The main component of the gas product was nitrogen. The majority of NH_3, which was a product of the decomposition of palladium tetrammine dichloride, was dissolved in the plating solution. The rest of the ammonia was removed by bubbling the gas through the 1-M HCl solution. Figure 4 shows the nitrogen flow rates for two successive platings

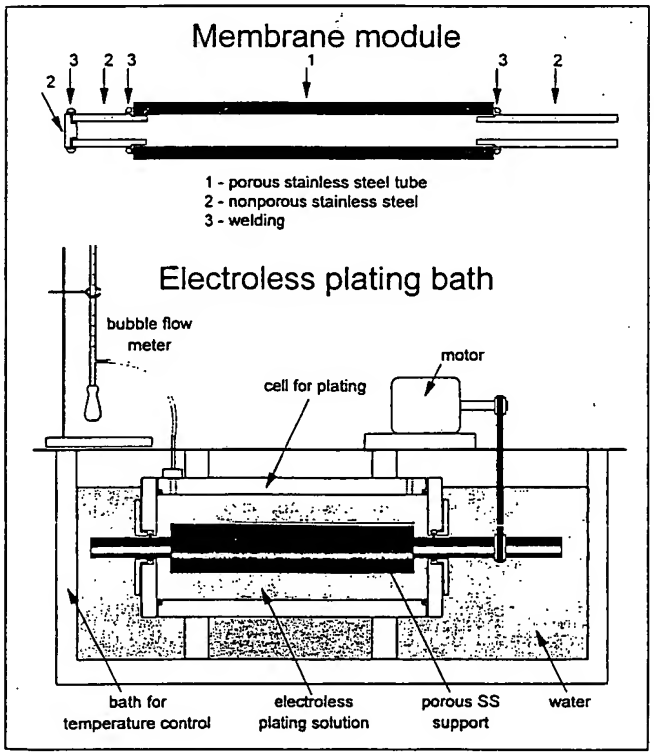

Figure 3. The membrane module and plating bath for the deposition of Pd on long porous stainless-steel tubes by the electroless-plating technique.

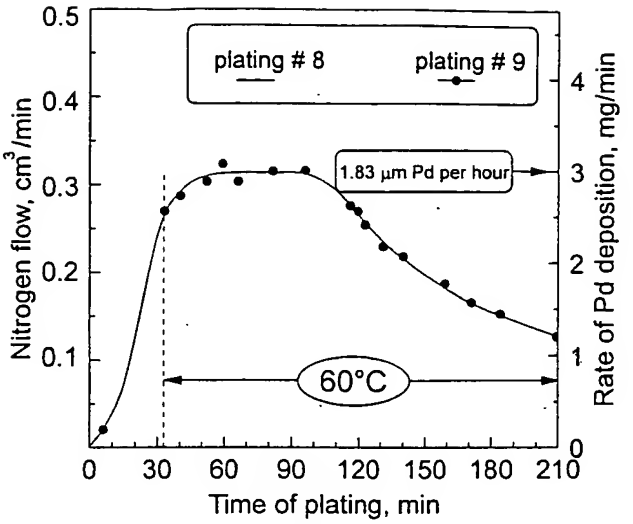

Figure 4. Variation of the nitrogen flow and rate of the palladium deposition with time of plating for two successive plating procedures.

(plating #8 and plating #9). The right axis presents the corresponding rate of the Pd deposition, which was estimated based on the ratio $2Pd/N_2$. The increase of the deposition rate during the first 30 min was caused by the changes of bath's temperature from 20°C to 60°C. After approximately one hour of steady-state deposition the activity of the plating decreased with the depletion of palladium ions, hydrazine, and the pH of the plating bath. A stable high rate of deposition for each plating was achieved by carefully rinsing the membrane between plating solutions. There is an excellent agreement between the quantity of the deposited palladium determined by the gas-flow measurement and the integration of these data, and by weighing of the support before and after the deposition.

The thickness of the Pd layer was determined from the plated amount and the density of Pd (12.0 g/cm^2). In some cases the thickness was estimated directly from the SEM picture. A total of eight membranes have been prepared and used for the various tests.

Permeation experiments

The permeation measurements of the initial PSS support and the membrane after deposition of the palladium layer were carried out using a stainless-steel membrane assembly. Figure 5 shows the experimental setup. The feed gas flowed upward through the outside of the membrane (shell side), and the permeant gas was collected on the tube side. A purge gas could also be used on the tube side, if desired. The upstream pressure was monitored by a capacitance pressure transducer and the permeate-side pressure was kept atmospheric. The gas permeation rate (the volumetric flow rate) was measured in the permeate side at atmospheric pressure and room temperature. A soap-bubble capillary flowmeter was used for flow rates less than 1 cm^3/min; a digital flowmeter (Alltech), for flow rates in the range of 1–200 cm^3/min; and a wet-test meter for flow rates greater than 200 cm^3/min. Temperature controllers (Omega CN-9000) were used to con-

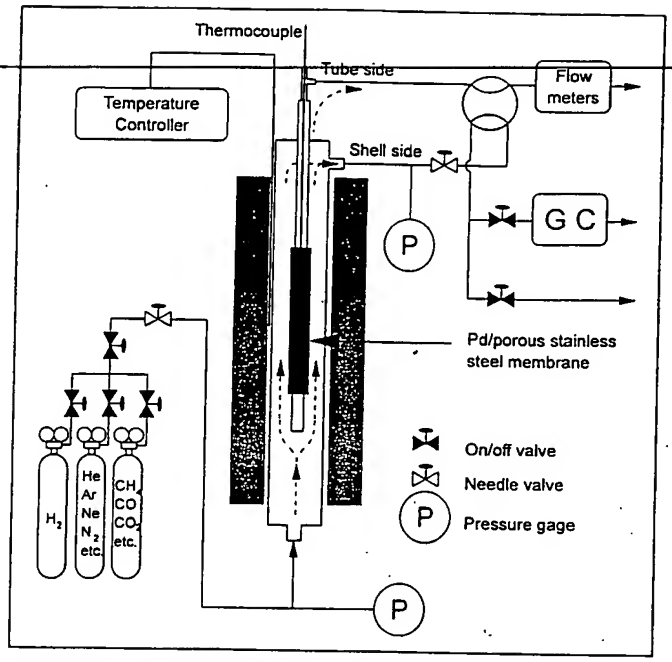

Figure 5. Experimental setup for permeation measurements.

trol the temperatures inside the furnace and inside the membrane module. The temperature variation along the membrane did not exceed 3°C.

To avoid hydrogen embrittlement the hydrogen fluxes were measured at temperatures greater than 300°C. Prior to the hydrogen permeation tests, the Pd/PSS membrane was heated in nitrogen or helium at a rate of about 1°C/min.

The fluxes of gases other than hydrogen (N_2, Ar, CO_2, CH_4, CO, Ne, He) were measured following a thorough purge of both shell and tube sides by the permeating gas. Without purging, a negative flux would be observed as a result of back diffusion of the dissolved hydrogen.

All the gases used had 99.9% or better purity except carbon dioxide (99.8%).

Structural characterization

The microstructure of the membranes was characterized by scanning electron microscopy (SEM, JEOL-840) and X-ray diffraction (XRD, Rigaku/USA D/MAX APD System) with Cu K_α radiation sources and graphite monochromators.

Results and Discussion

Permeability of the original support

Dense Pd membranes were successfully prepared when a top layer of stainless steel was mechanically removed prior to cleaning, activation, and palladium deposition. The influence of different mechanical treatments on the permeation characteristics of the original PSS support was studied. It was found that conventional machining and mechanical treatments (sandpaper, file, etc.) of PSS closed surface pores decreased their size and, consequently, reduced the porosity of the top layer, making the treated surface almost impermeable. For example, the nitrogen permeance of the PSS long tube dropped from ~200 to 0.2 $m^3/(m^2 \cdot h \cdot atm)$ after surface filing (Table 3). Therefore, the controlled machining or mechanical treatment can be used to decrease the pore size of the top layer of the PSS support. Electrical discharge machining can keep the surface pores open without changes in the pore size (Mott Metallurgical, 1995). Treatment by a stainless-steel brush yielded a small reduction in the PSS permeability. A subsequent cleaning by alkaline solution in an ultrasonic bath increased the permeability of PSS to within 20% of the value prior to the brush treatment (Table 3). The simplicity of the treatment by stainless-steel brush, compared with electrical discharge machining, motivated the choice of this treatment.

Table 3. Nitrogen Permeance of the Porous Stainless Steel

Sample No.	Treatment	Permeance (F), $m^3/(m^2 \cdot h \cdot atm)$
1	None	230.4
1	Stainless-steel brush	182.1
1	+ Cleaning solution	206.5
1	+ 10 M HCl, 5 min	207.0
1	+ Activation (× 8)	187.2
2	Sandpaper (intense)	49.4
2	+ Cleaning solution	71.0
2	+ 10 M HCl, 5 min	72.6
2	+ Activation (× 8)	29.3
3	File (intense)	0.2
3	+ 10 M HCl, 20 h	112

Table 3 also shows that the short-term treatment by concentrated hydrochloric acid did not change the pore size and porosity of the PSS, while extended contact with the acid can reopen mechanically closed surface pores as a result of dissolving the top layer of stainless steel.

An activated layer, with a thickness of about 1 μm, was responsible for the observed decrease in the PSS's permeability (Table 3). The change of the permeance was larger for #2, where the size of surface pores had been substantially decreased by the preliminary mechanical treatment.

Hydrogen flux and selectivity coefficient

The rate of hydrogen permeation or the hydrogen flux can be expressed as

$$J = \frac{Q}{L} \cdot (P^n - P_0^n) = F \cdot (P^n - P_0^n). \qquad (1)$$

A typical relation with $n = 0.5$ between the rate of hydrogen permeation and the transmembrane pressure difference is shown in Figure 6. The hydrogen fluxes of 3.2 and 6.8 $m^3/(m^2 \cdot h)$ at a pressure difference of 1 atm were measured at 350 and 500°C, respectively. These temperatures correspond to the permeances of 7.8 and 16.4 $m^3/(m^2 \cdot h \cdot atm^{0.5})$. The regression coefficient was usually around 0.999 for all the membranes tested (see Table 4). These results show that the dependence of the hydrogen solubility in Pd follows Sievert's law. Furthermore, the hydrogen diffusion through the bulk of the palladium film is the rate-determining step for hydrogen permeation.

An increase in the hydrogen flux can be achieved by decreasing the thickness of the palladium layer and increasing

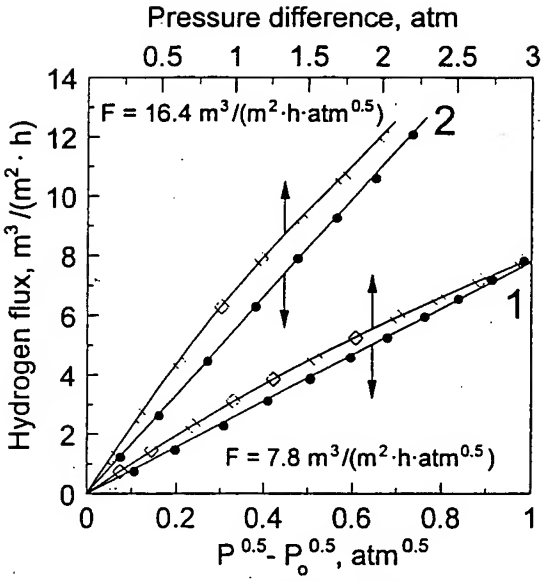

Figure 6. Influence of the pressure difference on the H_2 flux at (1) 350 and (2) 500°C.

the porosity of the support. The variation in the hydrogen fluxes with the porosity of the support for the same thickness of the Pd dense layer was discussed by Itoh et al. (1995). To deposit a thinner layer the pore size of the support should be smaller or should be decreased prior to the Pd deposition. Because of the differences between supports, such as effective porosity of the top layer and the diameter of the biggest pores, the thickness of Pd dense layer usually was varied from 19 to 28 μm and the hydrogen fluxes from 2 to 4 $m^3/(m^2 \cdot h)$ were measured at a pressure difference of 1 atm. A thinner dense Pd layer also can be prepared by predominant deposition of palladium inside the pores of the top layer of the support.

Permeation of a wide range of pure gases through the Pd/PSS membranes was also studied. At room temperature nitrogen or helium fluxes through the freshly prepared membranes were not detected in many cases at pressure difference up to 3 atm. This strongly indicated that the deposited palladium layer was defect free and impermeable to any gas except hydrogen.

Table 4. Hydrogen Permeance and the Value of the Pressure Exponent from the Different Procedures of Estimation

Memb. No.	Permeat. Temp. °C	Type of Procedure to Estimate Value of n*	n Pressure Exponent	Regress. Coeff.	Permeance $m^3/m^2 \cdot hr \cdot atm^n$
1	350	1	0.5	0.9991	7.934
		2	0.600	0.9998	6.220
		3	0.591	—	6.352
2	350	1	0.5	0.9993	3.928
		2	0.605	0.9999	3.036
		3	0.609	—	3.011
2	470	1	0.5	0.9985	7.1336
		2	0.646	0.9999	5.039
		3	0.635	—	5.158
2	500	1	0.5	0.9996	9.291
		2	0.434	0.9999	11.159
		3	0.443	—	10.856

*Procedure #1: $J = F \cdot (P^{0.5} - P_0^{0.5})$; procedure #2: $J = F \cdot (P^n - P_0^n) + B$; $\lim |B| \to 0$; procedure #3: $F = F_0 + A \cdot (P^n - P_0^n)$; $\lim |A| \to 0$.

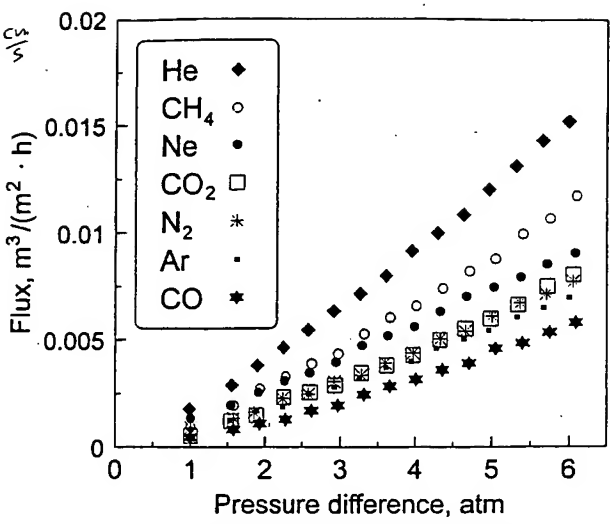

Figure 7. Flux of different gases as a function of the pressure difference at 350°C.

After increasing the temperature to 350°C in the nitrogen atmosphere, a very small nitrogen flux was detected. Figure 7 shows the fluxes of different gases other than hydrogen at 350°C as a function of the transmembrane pressure difference. Because of the very low permeability of the membrane for these gases, in many cases the fluxes could not be measured accurately at pressure differences less than 1 atm.

For all these gases, the fluxes increase exponentially with the pressure difference. Empirically, the fluxes could be described by Eq. 1, as has been done by Collins and Way (1993). They found that the exponent of the pressure, n, ranged from about 1.37 to 1.51 for helium and nitrogen. Another empirical way to express the variation of fluxes with the pressure difference is $J = F \cdot (P - P_0)^n$, with the value of n likewise being greater than 1.

There are at least two mechanisms involved in the transport process here: Knudsen diffusion and viscous or Poiseuille flow. For the Knudsen diffusion, permeance does not depend on the pressure difference, while for the viscous flow, the permeance should be proportional to the pressure. The viscous flow contribution is proportional to the average pressure across the membrane, which also determines the mean free path of the gas molecules. Therefore, for the same pressure difference, P_{ave} would be different for a different downstream pressure, P_0. Thus, it appears that there is no real physical basis for presenting such fluxes either as $J = F \cdot (P^n - P_0^n)$ or as $J = F \cdot (P - P_0)^n$.

For nonadsorbable gases, the total permeance can be expressed as the sum of the Knudsen flow and the viscous or Poiseuille flow (Uhlhorn et al., 1989):

$$F = F_k + F_v \cdot P_{ave} = \frac{2}{3}\sqrt{\frac{8}{\pi}} \cdot \frac{\epsilon \mu_k r}{L\sqrt{RTM}} + \frac{1}{8} \cdot \frac{\epsilon \mu_v r^2}{L \eta RT} \cdot P_{ave}. \quad (2)$$

The presence of surface flow should be taken into account if the pressure and temperature are such that gas adsorption

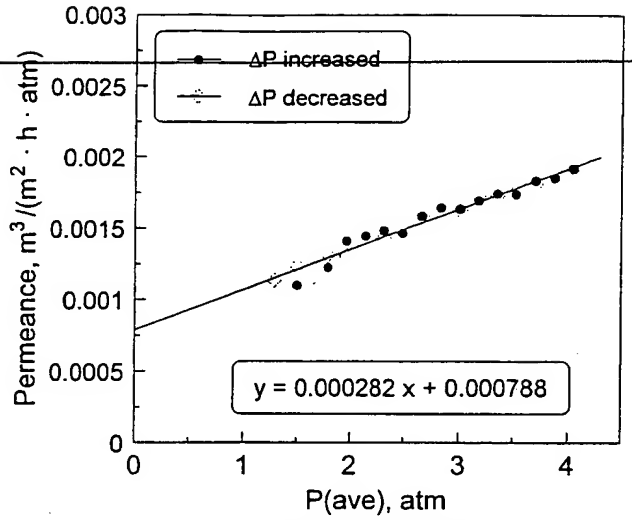

Figure 8. Methane permeance vs. average pressure across the membrane.

Circles: the pressure difference was consecutively increased; diamond: the pressure difference was consecutively decreased.

on the surface is significant. We can assume that for temperatures greater than 350°C, the contribution from the surface flow for He, Ne, Ar, N_2, CO_2, and CH_4 can be neglected. Equation 2 shows that a plot of F vs. P_{ave} should yield a straight line with the slope F_v and intercept F_k.

The permeances for all gases were plotted against the average pressure, P_{ave}, and the values of F_k and F_v were estimated. As an example, Figure 8 shows the methane permeation data as a function of the average pressure. To demonstrate the reproducibility of the permeation measurements, two sets of data are presented. The first (circles) illustrates the case where the pressure difference was consecutively increased from 1 to 6 atm, while the second set (diamonds) shows that the pressure was consecutively decreased in the same range of pressure differences. Since the data of both sets were so close, they were analyzed together. Intersection with axis Y gives the value of F_k, and the slope (F_v) indicates the contribution of the viscous flow to the total methane flow through the membrane. From Eq. 2 it can be seen that for a membrane at a given temperature, the F_k is inversely proportional to the square root of the molecular weight of the permeation gas, and F_v is inversely proportional to the viscosity of this gas at a given temperature.

The ideal separation factor, or selectivity coefficient (α^*), is defined as the ratio of the fluxes of two pure gases, i and j, as follows:

$$\alpha^*_{ij} = \frac{J_i}{J_j}. \tag{3}$$

The selectivity coefficients of gases—for example, argon—with respect to other gases, for pure Knudsen diffusion and for viscous flow, could be expressed by

$$\alpha^*_k(\text{Ar/gas}) = \frac{\sqrt{M_{gas}}}{\sqrt{M_{Ar}}} \tag{4}$$

and

$$\alpha^*_v(\text{Ar/gas}) = \frac{\eta_{gas}}{\eta_{Ar}}, \tag{5}$$

respectively. The expected Ar selectivity coefficients for pure Knudsen diffusion, α^*_k, and for pure viscous flux, α^*_v, were calculated using Eqs. 4 and 5, respectively, and compared with the estimation from the experimental data as ratios $F_k(\text{Ar})/F_k(\text{gas})$ and $F_v(\text{Ar})/F_v(\text{gas})$, as shown in Figure 9a and 9b. The values of viscosity, η, for He, Ne, Ar, N_2, CO_2, and CH_4 at 350°C were calculated based on the data presented in the literature (Lide, 1996). The values of α^*_k and α^*_v obtained from the experimental data are very close to the values obtained from Eqs. 4 and 5.

The radius of pores can be approximately estimated based on the experimental ratio of F_v/F_k and on the assumption that the geometrical factors of a porous medium are the same for Knudsen diffusion and viscous flow:

$$\frac{F_v}{F_k} = \frac{3}{16}\sqrt{\frac{\pi}{8}} \cdot \frac{1}{\sqrt{RT}} \cdot \frac{\sqrt{M}}{\eta} \cdot r. \tag{6}$$

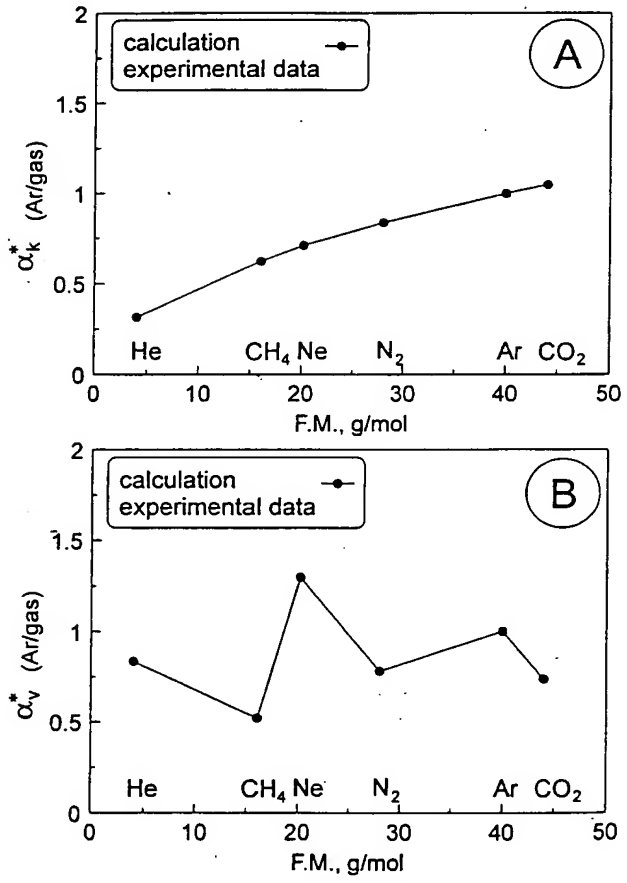

Figure 9. Expected selectivity coefficients (Ar/gas): (A) for pure Knudsen diffusion calculated from Eq. 4 vs. those estimated from experimental data as the ratio $F_k(\text{Ar})/F_k(\text{gas})$; (B) for pure viscous flux calculated from Eq. 5 with those estimated from the experimental data as the ratio of $F_v(\text{Ar})/F_v(\text{gas})$ T=350°C.

In the strict sense, the assumption that μ_k and μ_v are the same is not correct. The geometric factor μ_v is inversely related to tortuosity, τ: $\mu_v = 1/\tau$. The geometric factor for Knudsen diffusion includes not only tortuosity, but reflection factor, θ_k, as well: $\mu_k = 1/(\tau \cdot \theta_k)$. The reflection factor is proportional to the roughness of the wall of pores. For smooth walls, θ_k equals 1; for a rough surface, where the diffuse reflection of molecules takes place after collision with the wall, θ_k is greater than 1 (a detailed description of the geometric aspects can be found in Burggraaf, 1996). The exact value of τ should be θ_k times lower than that estimated from Eq. 6. At the same time, in our case, the roughness of the pore walls is determined by the roughness of the Pd grains, which is very low. The recrystallization texture and aggregation of the Pd grains is discussed later. It is then reasonable to assume that θ_k is close to 1 and $\mu_k \cong \mu_v = 1/\tau$. Thus, for $T =$ 350°C Eq. 6 can be rewritten as

$$\frac{F_v}{F_k} = 1.632 \times 10^{-3} \cdot \frac{\sqrt{M}}{\eta} \cdot r. \tag{7}$$

As shown in Figure 10, a plot of the ratio of F_v/F_k vs. $\sqrt{M}/\eta$ should be a straight line whose slope should yield the value of the pore radius, r, which in this case is 0.38 μm. Considering the extremely low measured fluxes, it appears that the observed scattering of r is reasonable.

Using this average value of r, the porosity of the palladium layer was calculated as

$$\epsilon = 8 \cdot L \cdot \eta \cdot \tau \cdot RT \cdot F_v \cdot \frac{1}{r^2}. \tag{8}$$

The tortuosity factor, τ, is most likely to be between 3 and 4. Therefore, a value of 3.5 was used in the calculations. From the value of porosity and assuming a uniform distribution and cylindrical shaped pores, the number of pores (N) per unit area (S) and the distance between their centers (l) were calculated according to

$$N = \frac{\epsilon \cdot S}{\pi r^2} \tag{9}$$

$$l = \frac{\sqrt{S}}{\sqrt{N}}. \tag{10}$$

The calculated values of ϵ, N, and l are 1.79×10^{-7}, 0.39 per 1 mm^2, and 1.61 mm, respectively.

The number of holes or pore entrances in the top layer of the PSS, which have an average diameter of 20–30 μm shown in Figure 1, is around 40 ± 10 per 1 mm^2. To estimate the dimension of the pores and the pore-size distribution on the outer surface of the original PSS, computer-controlled scanning electron microscopy (CCSEM, RJ Lee Group, Inc., 530 McCormick St., San Leonardo, CA) was used. In CCSEM the backscattered electron mode, which is sensitive to differences in atomic number, is used to determine when the electron beam is in the pore. When a pore is located, the computer drives the beam in a preset pattern to determine the dimensions of the pore. The measurements performed by the RJ Lee Group indicated that the largest pores, with a diameter in the range between 7 and 8 μm, made up about 1% of all pores. Based on the assumption of a uniform distribution of pores, therefore, we can conclude that the number of pores with large openings (20–30 μm) at one end (at the surface of PSS), but narrowing to 7–8 μm at the other end, is roughly 0.4 ± 0.1 per 1 mm^2. This is in good agreement with the value of N, 0.39 per 1 mm^2, calculated from Eq. 9. Thus, the pore gaps generated in the Pd layer while heating the membrane to 350°C are more likely to be located above such pores. Excessive tension exists in the Pd layer at points above these pores at high temperatures and causes the appearance of pore gaps, which reduce this tension. To decrease the probability of the creation of pore gaps, a thicker Pd layer should be deposited, or the pore entrances, as well as the large pores, should be blocked prior to the activation and deposition. Another way to prevent the creation of pore gaps is, as was mentioned before, the deposition of predominantly Pd inside the pores of the top layer.

Since the pressure dependence of the hydrogen flux is different from all other gases, the selectivity coefficient between

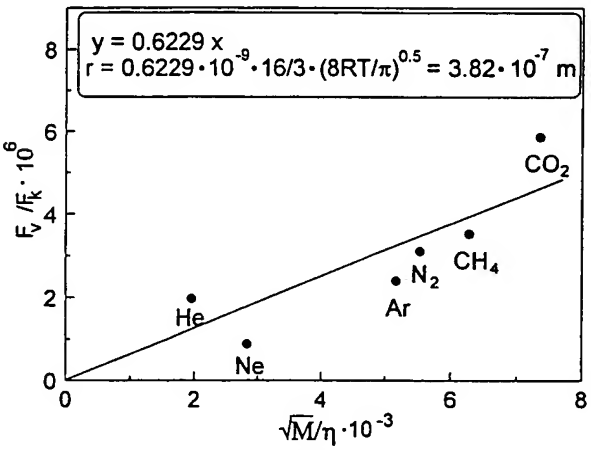

Figure 10. Variation of the ratio F_v/F_k as a function of $\sqrt{M}/\eta$.

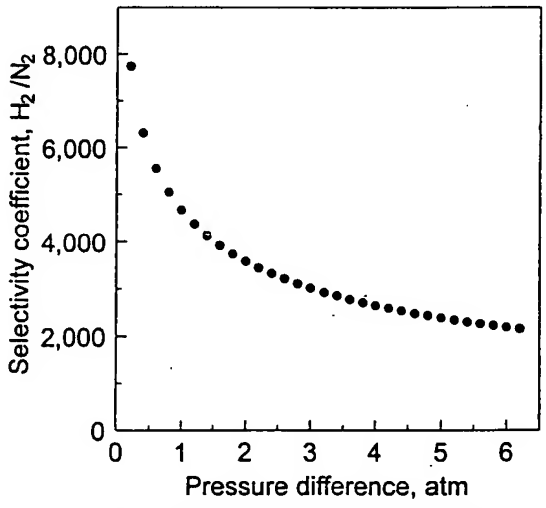

Figure 11. H_2/N_2 selectivity coefficient as a function of the pressure difference at 350°C (based on the experimental data).

hydrogen and other gases depends on the pressure differences, as shown in Figure 11 for nitrogen. The H_2/N_2 selectivity coefficients for other prepared membranes at 350°C and a pressure difference of 1 atm, ranged from 600 to 5,000.

Temperature dependence of membrane performance

Figure 12 shows a variation of the hydrogen and nitrogen fluxes with the temperature at pressure differences of 0.5, 1, 1.5 and 2 atm. In this experiment the temperature was increased from 350°C to 700°C and the membrane was held at each temperature for about 5 h. Temperatures greater than 700°C were not applied due to the large reduction in hydrogen flux and the considerable increase in nitrogen flux.

For such a membrane temperature history, the permeation data reflect the influence of the temperature on both fluxes and the reorganization of the membrane structure. As expected, an increase in temperature leads to an increase in hydrogen flux. The drop in fluxes at temperatures greater than 550°C was most likely caused by an intermetallic diffusion. At temperatures greater than 550°C similar deterioration in the hydrogen permeation rate was observed for all membranes prepared in this manner.

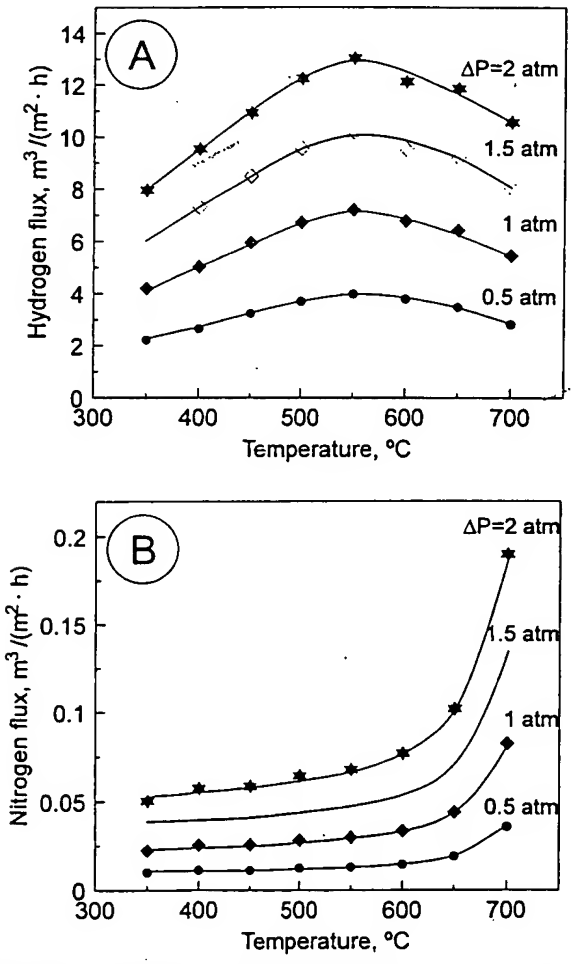

Figure 12. Influence of temperature on H_2 (A) and N_2 (B) fluxes for different ΔP; temperature was increased from 350°C to 700°C.

The value of the exponent of the pressure, n, is routinely used as an indication of the rate-limiting step of the hydrogen permeation through the Pd layer. If the value of n is equal to 0.5, Sievert's law is assumed to be followed (Hurlbert and Konecny, 1961). An increase in n will result when the permeation rate is influenced by the surface process, leakage of the hydrogen through defects in the Pd layer, transport resistance of the support, poisoning of the palladium surface, and so forth. Collins and Way (1993) mentioned that n also depends on the temperature. The same assumption was made by Hurlbert and Konecny (1961). They found that for the palladium film with thickness ≥ 20 μm and at 350°C the value of n is 0.68, and they concluded that with increasing temperature, the value of n should probably decrease to the limiting value 0.5.

The value of n, which best fits the permeation data, was estimated. Two procedures are commonly used to estimate the optimum value of n: J is plotted against $(P^n - P_0^n)$, $J = F \cdot (P^n - P_0^n) + B$, $\lim |B| \to 0$; and F is plotted against $(P^n - P_0^n)$, $F = F_0 + A \cdot (P^n - P_0^n)$, $\lim |A| \to 0$. It was found that in some cases the optimum value of n was indeed lower at higher temperatures, as was mentioned by Hurlbert and Konecny (1961) and Collins and Way (1993), but such a correlation was not always valid. As an example, Table 4 gives n, F, and regression coefficient, R^2, for different membranes at different temperatures of measurements (the differences in permeances are mainly due to the different quality of the support). The goodness of fit is relatively insensitive to the value of n. A good fit does not necessarily prove that this value of n reflects the quality of the membrane or could be used to reach a conclusion about the rate-limiting step of the hydrogen permeation, especially if the value is in the range between 0.4 and 0.6. Therefore, the optimum value of n is too sensitive to the accuracy of the permeation measurements to be used without a great care.

Significant increases in the pressure exponent up to 0.8–0.9 were observed only at the temperatures around 700°C. This increase in n was caused by the degradation of the membrane and accompanied by a 4-fold increase of the nitrogen flux. The increase of the nitrogen flux with the temperature (Figure 12b), contrary to the theory (Eq. 2), was due to the modification of the morphology of the Pd layer.

Intermetallic diffusion is a severe problem for the application of the palladium membranes at high temperatures because of the decline of the hydrogen flux. It is well known that a considerable thermal vibration occurs in the metal lattice at the Tamman temperature that is equal to 0.5 of its melting temperature (in K). If there is an interface between two metals, this thermal vibration enormously increases the mobility of metal atoms and their capability for diffusion. Palladium and stainless steel have melting points of 1,552 and 1,375–1,400°C, respectively. The corresponding Tamman temperatures are about 640 and 550–560°C. We could therefore expect that at temperatures around 550°C the diffusion of stainless-steel components into the palladium layer should take place. An alloy of Pd with the SS components created under such circumstances would have lower hydrogen fluxes. This reasoning is in very good agreement with the data presented in Figure 12a. Moreover, Gryaznov et al. (1993) showed by XPS that stainless-steel components indeed diffused into the palladium layer. Thus, the lowest Tamman

temperature of the metal–metal couple determines the temperature where substantial intermetallic diffusion occurs.

One way to prevent such diffusion is the creation of an additional thermostable oxide layer between the Pd layer and the support. Edlund and Pledger (1993) successfully prepared composite membrane $Pd/SiO_2/V/SiO_2/Pt$, which maintained good thermal stability. Edlund and McCarthy (1995) later reported membrane stability for up to 80 h at 700°C for their composite Pd/V membrane with nonwoven aluminum oxide felt as an intermediate layer. Gryaznov et al. (1993) showed that the best resistance to intermetallic diffusion between PSS and Pd, deposited by magnetron sputtering, are zirconia, magnesia, tantalum oxide, and tungsten. Tungsten can be used as an intermediate layer because of its extremely high melting temperature and, consequently, high Tamman temperature of about 1,570°C.

If the membrane has been treated at high temperatures prior to the permeation experiments, and the temperature did not exceed the temperature of intermetallic diffusion, the measured fluxes of hydrogen and nitrogen depended only on the temperature. Under the current condition the membrane performance should not be affected by the reorganization of the palladium layer. The hydrogen and nitrogen flux as a function of the temperature for the membrane initially treated at 500°C for 5 h is presented in Figure 13. In agreement with the theory, the nitrogen flux decreases as the temperature increases. The increase in the hydrogen flux and the decrease in the nitrogen flux with temperature result in an increase in the selectivity coefficient at high temperatures. According to the data presented in Figure 13, at 1-atm pressure difference the selectivity coefficient changed from 1,390 at 350°C to 3,350 at 470°C.

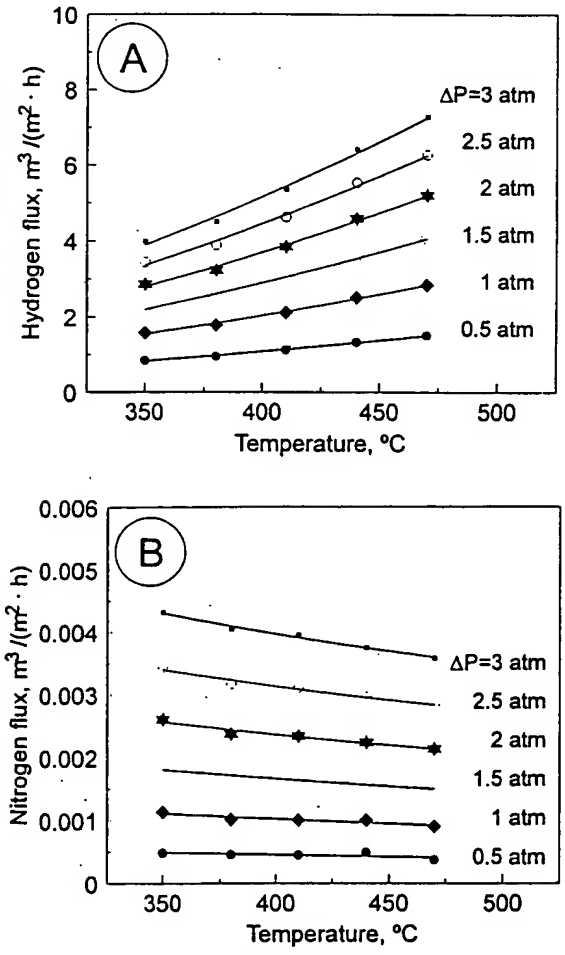

Figure 13. Influence of temperature on H_2 (A) and N_2 (B) fluxes for different ΔP; temperature was decreased from 500°C to 350°C.

The experimental values of the hydrogen permeances at different temperatures were used to estimate the activation energy for hydrogen permeation through the membrane. The permeability depends on the temperature, as

$$Q = Q_0 \cdot \exp\left(-\frac{E}{RT}\right). \tag{11}$$

This equation is correct when the value of n does not depend on the temperature. For all temperatures $n = 0.5$ was used. Figure 14 shows an Arrhenius relation between the rate of hydrogen permeance and the temperature. The activation energy of the composite membrane for hydrogen permeation, calculated from this graph, is 16.4 kJ/mol. Similar activation energy of 19.7 kJ/mol was reported earlier (Mardilovich et al., 1996b) for a different membrane. These values are in agreement with those for Pd membranes reported previously: 14.45 kJ/mol for 17 μm Pd film on ceramic support (Collins and Way, 1993); and 23 kJ/mol for 0.3 μm Pd/Ag film on ceramic support (Jayaraman and Lin, 1995). In the later case, since a hydrogen-to-nitrogen selectivity coefficient as low as 5.7 was reported, it is difficult to assess the quality of the membrane. Furthermore, the hydrogen fluxes were studied only in the range of temperature from 100 to 250°C.

Long-term stability

Pd/PSS membranes must demonstrate long-term stability if they are to be viable for industrial applications. The membranes were tested at 350°C for up to 1100 h. Figure 15 shows permeation measurements through the membrane at 350°C

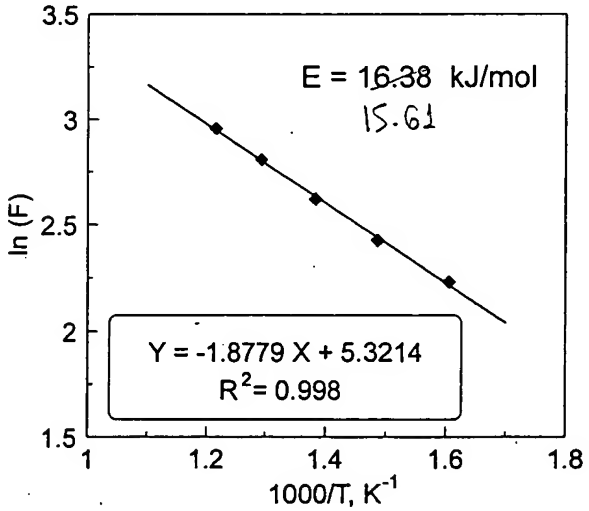

Figure 14. Arrhenius relation between the hydrogen permeance and the temperature.

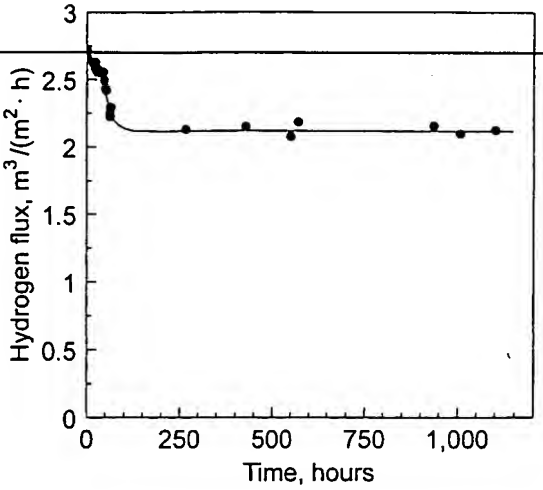

Figure 15. Hydrogen flux vs. time: $P = 2$ atm; $P_0 = 1$ atm; $T = 350$°C.

over a period of 1,100 h. During this period of time the hydrogen partial pressure difference varied from 0.1 to 6 atm and fluxes of many other gases and mixtures, such as N_2, Ar, He, CO_2, CH_4, N_2/H_2, CO_2/H_2, were also measured. No significant changes of the membrane performance were observed, except for the initial decrease of the hydrogen flux. The decline in the hydrogen flux over the first ~ 50 h is more likely the result of rearrangement of the Pd/PSS interface with the rest of the activated layer. Under high temperatures and in the presence of hydrogen this layer becomes denser and the local, effective porosity of the support's top layer is decreased, resulting in the loss of effective membrane area.

Figure 16 shows SEM photographs of Pd/PSS membranes exposed at 350°C for 5 and 1,100 h. After 1,100 h, the distribution of the Pd crystal orientation is nonrandom. From the XRD data presented in Figure 17, it can be seen that the preferred orientation is (111). A recrystallization-texture has been developed by a recrystallization process that is also accompanied by the aggregation of grains. After 1,100 h at 350°C, some of the grains are as large as 5 μm. According to the XRD data the size of the initial Pd grains just after deposition is around 20 nm (calculations were made by JADE software, MDI Material Data Inc., using the Debye–Scherrer equation). Treatment of the Pd/PSS membrane at 700°C leads to the additional reorganization of the palladium texture. Figure 17 shows that the Pd membrane treated at 700°C has a predominantly (200) crystal orientation.

The Pd lattice parameter, a_0, was found to be 3.887 Å, 3.894 Å, 3.893 Å, and 3.894 Å for the original membrane, the membrane treated at 350°C for 5 and 1100 h, and the membrane treated at 700°C for 5 h, respectively. Lattice parameters were estimated by plotting the value of a, calculated for each reflection at 2θ up to 130°, against $\sin^2\theta$ and extrapolation to a value a_0 at $\theta = 90°$ (Cullity, 1988). The recrystallization of the deposited palladium at 350°C , and the treatment at 700°C do not appear to lead to any significant changes of the lattice. The parameters for Pd treated at 350°C and higher are very close to the a_0 for pure Pd as reported in the literature ($a_0 = 3.8898$ Å: Berry, 1974) and to that estimated in this study using a Pd sheet ($a_0 = 3.891$ Å: XRD pattern of Pd sheet presented in Figure 17, curve 5).

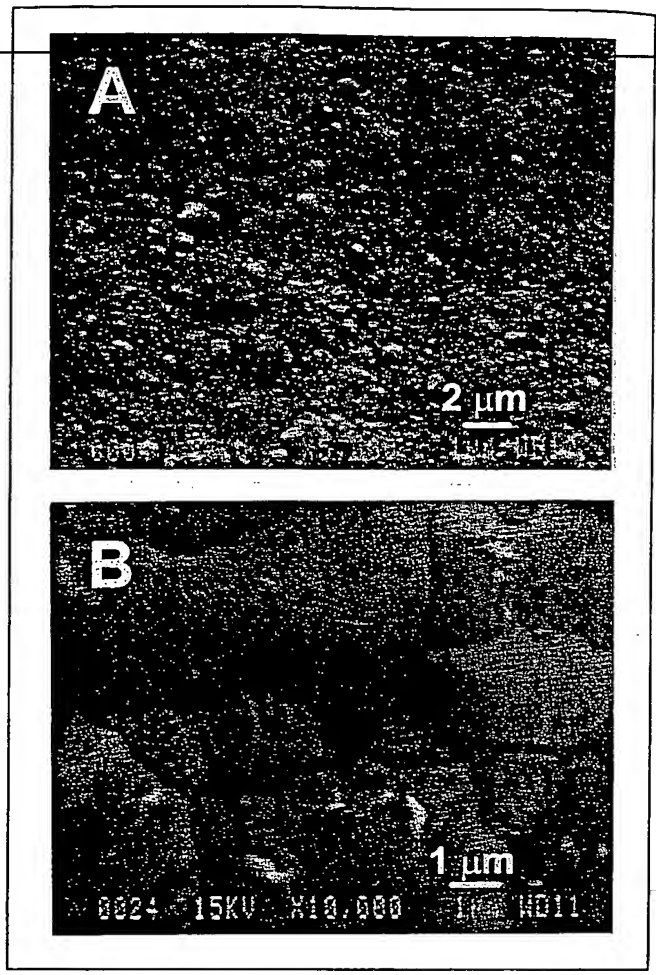

Figure 16. Surface morphology of the Pd/porous stainless-steel membrane after exposure at 350°C for (A) 5 and (B) 1,100 h.

Based on the data presented here and in the previous paragraph, we can conclude that the prepared membranes can withstand brief operation at temperatures up to 500–550°C. For long-term exposures, a more appropriate temperature range is from around 300°C to 450°C. The minimum operating temperature of 300°C for pure Pd is defined by hydrogen embrittlement, a phenomenon when the β palladium hydride may nucleate from the α phase. This causes loss in density in the Pd layer and the selectivity of the membrane as a result of alternative Pd lattice expansion and reduction (Saracco and Specchia, 1994; Shu et al., 1991).

Conclusions

The results of this research show that the electroless plating technique can produce a dense Pd layer on long, porous stainless-steel tubes with pores up to 8 μm. At room temperature the nitrogen or the helium fluxes through such membranes were not detected at pressure differences up to 3 atm. The thickness of the dense Pd layer strictly depended on the diameter of the largest pores in the support.

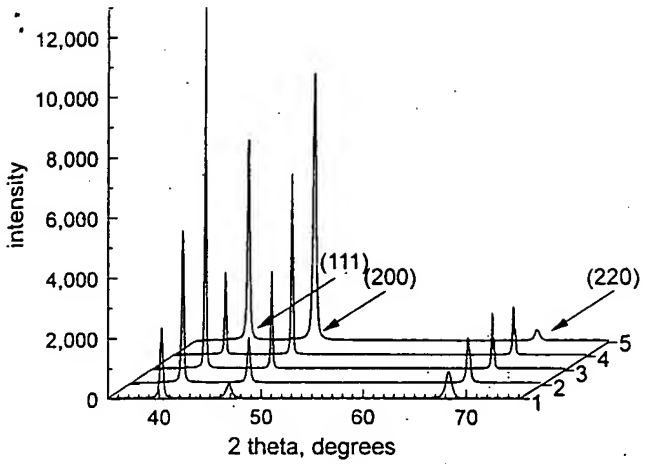

Figure 17. XRD of the initial Pd/porous stainless-steel membrane (1); membrane after exposure at 350°C for 5 h (2) and 1,100 h (3); after exposure at 700°C for 5 h (4), and a sheet of pure Pd (5).

At 350°C the developed membranes with a palladium layer of ~ 20 μm exhibited hydrogen permeances up to 8 $m^3/(m^2 \cdot h \cdot atm^{0.5})$. At a pressure difference of 1 atm and 350°C selectivity coefficients (H_2/N_2) as high as 5000 and hydrogen fluxes up to 4 $m^3/(m^2 \cdot h)$ were observed. The selectivity coefficient rose with the temperature increase and the decrease in pressure difference.

The contribution of viscous flux was taken into account to explain the transport mechanism of gases other than hydrogen through the membranes. It was found that these gases pass through the pore gaps in the palladium layer. These pore gaps are most likely created during thermal treatment to reduce the excessive tension at the points located above the 7–8-μm pores with large (20–30 μm) openings at the surface of the PSS. Their low-density (less than 1 per 1 mm^2) gives low values of the permeance through the gaps [around 0.001 $m^3/(m^2 \cdot h \cdot atm)$]. These fluxes could be decreased further by the deposition of a thicker Pd layer or by partial blocking of the big PSS pores prior to activation and deposition.

The long exposure (1,100 h and more) of the membrane to hydrogen at 350°C led to the recrystallization texture. The (111) orientation became preferred, and aggregation of the palladium grains occurred. The hydrogen flux did not vary significantly in time. At temperatures of 550°C and higher, the membranes could withstand only brief operation without appreciable changes in the hydrogen flux and selectivity, because of the intermetallic diffusion.

The Pd membranes that were developed show themselves to be extremely promising for practical applications in the range of temperatures from ~ 300 to 450°C.

Acknowledgment

We gratefully acknowledge the financial support provided by China Technical Consultants, Inc., Taipei, Taiwan, R.O.C.

Notation

E = activation energy, J/mol
F = rate of gas permeation per unit area and per unit of a transmembrane pressure difference, or permeance, $mol/m^2 \cdot s \cdot Pa^n$ or $m^3/m^2 \cdot h \cdot atm^n$
F_k = permeance due to Knudsen diffusion, $mol/m^2 \cdot s \cdot Pa$
F_v = permeance divided by pressure due to viscous or Poiseuille flow, $mol/m^2 \cdot s \cdot Pa^2$
J = rate of gas permeation per unit area, or flux, $mol/m^2 \cdot s$ or $m^3/m^2 \cdot h$
L = thickness of the Pd layer, m
M = molecular mass of the gas, kg/mol or g/mol
P = upstream pressure, Pa or atm
R = gas constant, J/mol · K (= 8.315)

Literature Cited

Athayde, A. L., R. W. Baker, and P. Nguyen, "Metal Composite Membranes for Hydrogen Separation," *J. Memb. Sci.*, **94**, 299 (1994).

Berry, L. G., ed., *Powder Diffraction File, 4-783 and 5-0681*, Joint Committee of Powder Diffraction Standards, PA (1974).

Bryden, K. J., and J. Y. Ying, "Nanostructured Palladium Membrane Synthesis by Magnetron Sputtering," *Mater. Sci. Eng.*, **A204**, 140 (1995).

Burggraaf, A. J., "Transport and Separation Properties of Membranes with Gases and Vapors," *Fundamentals of Inorganic Membrane Science and Technology*, A. J. Burggraaf and L. Cot, eds., Elsevier, Amsterdam, The Netherlands, p. 331 (1996).

Buxbaum, R. E., and T. L. Marker, "Hydrogen Transport Through Non-porous Membranes of Palladium-Coated Niobium, Tantalum and Vanadium," *J. Memb. Sci.*, **85**, 29 (1993).

Buxbaum, R. E., and A. B. Kinney, "Hydrogen Transport Through Tubular Membranes of Palladium-Coated Tantalum and Niobium," *Ind. Eng. Chem. Res.*, **35**, 530 (1996).

Collins, J. P., and J. D. Way, "Preparation and Characterization of a Composite Palladium-Ceramic Membrane," *Ind. Eng. Chem. Res.*, **32**, 3006 (1993).

Cullity, B. D., *Elements of X-Ray Diffraction*, Addison-Wesley, Reading, MA (1978).

Edlund, D. J., and J. McCarthy, "The Relationship Between Intermetallic Diffusion and Flux Decline in Composite-Metal Membranes: Implications for Achieving Long Membrane Lifetime," *J. Memb. Sci.*, **107**, 147 (1995).

Edlund, D. J., and W. A. Pledger, "Thermolysis of Hydrogen Sulfide in a Metal-Membrane Reactor," *J. Memb. Sci.*, **77**, 255 (1993).

Govind, R., and D. Atnoor, "Development of a Composite Palladium Membrane for Selective Hydrogen Separation at High Temperature," *Ind. Eng. Chem. Res.*, **30**, 591 (1991).

Gryaznov, V. M., O. S. Serebryannikova, M. Yu. Serov, M. M. Ermilova, A. N. Karavanov, A. P. Mischenko, and N. V Orekhova, "Preparation and Catalysis over Palladium Composite Membranes," *Appl. Catal. A: General*, **96**, 15 (1993).

Honma, H., and K. Kanemitsy, "Electroless Nickel Plating on Alumina Ceramics," *Plat. Surf. Finish.*, 62 (1987).

Hurlbert, R. C., and J. O. Konecny, "Diffusion of Hydrogen through Palladium," *J. Chem. Phys.*, **34**, 655 (1961).

Hybertson, B. M., B. N. Hansen, R. M. Barkley, and R. E. Sievers, "Deposition of Palladium Films by a Novel Supercritical Fluid Transport-Chemical Deposition Process," *Mater. Res. Bull.*, **26**, 1127 (1991).

Itoh, N., T.-H. Wu, and K. Haraya, "Two- and Three-Dimensional Analysis of Diffusion Through a Dense Membrane Supported on a Porous Material," *J. Memb. Sci.*, **99**, 175 (1995).

Jayaraman, V., and Y. S. Lin, "Synthesis and Hydrogen Permeation Properties of Ultrathin Palladium-Silver Alloy Membranes," *J. Memb. Sci.*, **104**, 251 (1995a).

Jayaraman, V., Y. S. Lin, M. Pakala, and R. Y. Lin, "Fabrication of Ultrathin Metallic Membranes on Ceramic Supports by Sputter Deposition," *J. Memb. Sci.*, **99**, 89 (1995b).

Kikuchi, E., and S. Uemiya, "Preparation of Supported Thin Palladium-Silver Alloy Membranes and Their Characteristics for Hydrogen Separation," *Gas Sep. Purif.*, **5**, 261 (1991).

Konno, M., M. Shindo, S. Sugawara, and S. Saito, "A Composite Palladium and Porous Aluminum Oxide Membrane for Hydrogen Gas Separation," *J. Memb. Sci.*, **37**, 503 (1988).

Li, Z. Y., H. Maeda, K. Kusakabe, S. Morooka, H. Anzai, and S. Akiyama, "Preparation of Palladium-Silver Alloy Membranes for Hydrogen Separation by the Spray Pyrolysis Method," *J. Memb. Sci.*, **78**, 247 (1993).

Lide, D. R., ed., *Handbook of Chemistry and Physics*, 77th ed., CRC Press, Boca Raton, FL (1996).

Mardilovich P. P., P. V. Kurman, A. N. Govyadinov, I. P. Mardilovich, M. M. Ermilova, N. V. Orekhova, A. N. Krivoshanova, R. Paterson, and V. M. Gryaznov, "Gas Permeability of Anodized Alumina Membranes with a Palladium-Ruthenium Alloy Layer," *Russ. J. Phys. Chem.*, **70**, 514 (1996a).

Mardilovich, P. P., Y. She, M.-H. Rei, and Y. H. Ma, "Permeation Characterization of Defect Free Pd/Porous Stainless Steel Membranes," Int. Conf. on Inorganic Membranes, Gatlinburg, TN (1996b).

McBride, R. B., and D. L. McKinley, "A New Hydrogen Recovery Route," *Chem Eng. Progr.*, **61**(3), 81 (1965).

Melashschenko, N. F., *Galvanic Coatings of Dielectrics*, Belarus, Minsk (1987).

Morooka, S., S. Yan, S. Yokoyama, and K. Kusakabe, "Palladium Membrane Formed in Macropores of Support Tube by Chemical Vapor Deposition with Crossflow Through a Porous Wall," *Sep. Sci. Technol.*, **30**, 2877 (1995).

Mott Metallurgical Corporation or Newmet Krebsoge, Inc., Manufacturer literature, (1995).

Peachey, N. M., R. C. Snow, and R. C. Dye, "Composite Pd/Ta Metal Membranes for Hydrogen Separation," *J. Memb. Sci.*, **111**, 123 (1996).

Saracco, G., and V. Specchina, "Catalytic Inorganic-Membrane Reactors: Present Experience and Future Opportunities," *Catal. Rev.-Sci. Eng.*, **36**(2), 305 (1994).

Shu, J., B. P. A. Grandjean, A. Van Neste, and S. Kaliaguine, "Catalytic Palladium-Based Membrane Reactors: Review," *Can. J. Chem. Eng.*, **69**, 1036 (1991).

Shu, J., B. P. A. Grandjean, E. Ghali, and S. Kaliaguine, "Simultaneous Deposition of Pd and Ag on Porous Stainless Steel by Electroless Plating," *J. Memb. Sci.*, **77**, 181 (1993).

Uemiya, S., Y. Kude, K. Sugino, N. Sato, T. Matsuda, and E. Kikuchi, "A Palladium/Porous-Glass Composite Membrane for Hydrogen Separation," *Chem. Lett.*, **10**, 1687 (1988).

Uemiya, S., N. Sato, H. Ando, Y. Kude, T. Matsuda, and E. Kikuchi, "Separation of Hydrogen Through Palladium Thin Film Supported on a Porous Glass Tube," *J. Memb. Sci.*, **56**, 303 (1991a).

Uemiya, S., T. Matsuda, and E. Kikuchi, "Hydrogen Permeable Palladium-Silver Alloy Membrane Supported on Porous Ceramics," *J. Memb. Sci.*, **56**, 315 (1991b).

Uhlhorn, R. J. R., K. Keizer, and A. J. Burggraaf, "Gas and Surface Diffusion in Modified γ-Alumina Systems," *J. Memb. Sci.*, **46**, 225 (1989).

Yan, S., H. Maeda, K. Kusakabe, and S. Morooka, "Thin Palladium Membrane Formed in Support Pores by Metal-Organic Chemical Vapor Deposition Method and Application to Hydrogen Separation," *Ind. Eng. Chem. Res.*, **33**, 616 (1994).

Yeung, K. L., and A. Varma, "Novel Preparation Techniques for Thin Metal-Ceramic Composite Membranes," *AIChE J.*, **41**, 2131 (1995).

Yeung, K. L., R. Aravin, J. Szegner, and A. Varma, "Metal Composite Membranes: Synthesis, Characterization and Reaction Studies," *Stud. Surf. Sci. Catal.*, **101**, 1349 (1996).

Manuscript received June 30, 1997, and revision received Sept. 29, 1997.

Exhibit B

Exhibit B

SEPARATIONS

Hydrogen Transport through Tubular Membranes of Palladium-Coated Tantalum and Niobium

Robert E. Buxbaum* and Andrew B. Kinney

Chemical Engineering Department, Michigan State University, East Lansing, Michigan 48824, and REB Research & Consulting, 25451 Gardner, Oak Park, Michigan 48237

Palladium-based membranes have been used for decades in hydrogen extraction because of their high permeability and good surface properties and because palladium, like all metals, is 100% selective for hydrogen transport. We describe experiments with hydrogen-extraction membranes made of palladium-coated niobium and tantalum heat-exchanger tubes. The cost was about \$45/ft of $^3/_8$ in. tubular membrane, and the fluxes were as high as 0.001 47 mol/m^2 s Pa$^{1/2}$ at 420 °C. The main transport resistance is in the refractory metal substrate. Durability tests showed a 15% reduction in flux for 31 days of continuous membrane operation. Assuming durability is maintained for at least 1 year, this price and flux should allow competitive application for hydrogen recovery in petrochemical plants and for membrane reactors.

Introduction

Palladium membranes have been used for decades to provide very pure hydrogen for semiconductor manufacture, fuel cells, and laboratory use. Palladium combines excellent hydrogen transport and discrimination properties with resistance to high temperatures, corrosion, and solvents. Further, palladium is easily formed into tubes that are easily fabricated into hydrogen extraction units[1,2] and palladium surfaces are not readily poisoned by carbon monoxide, steam, and hydrocarbons.[1,3,27] These properties would make palladium membranes very attractive for use with petrochemical gases except that palladium and its alloys are expensive and soft. Membrane units must employ thick-walled tubes costing \$3000/ft^2 or more. Further, the thick wall lowers the hydrogen flux since flux is inversely proportional to membrane thickness. Thus, despite their advantages, palladium−alloy membranes are usually too expensive for large-scale hydrogen recovery and membrane reactors.

Developmental History of Composite Metal Membranes

As Figure 1 shows, several low-cost refractory metals have greater hydrogen permeabilities than palladium. These metals, including niobium, tantalum, and vanadium, are also stronger than palladium and are easily fabricated into tubes and other useful shapes. Thin-walled tubes of these metals would show very high hydrogen fluxes at a fraction of the cost of palladium, but until recently their poor surface properties reduced transport dramatically.[4−13]

In 1967, Makrides et al. at Harvard University[4] patented a hydrogen-extraction membrane where a refractory metal was coated with palladium to facilitate hydrogen ingress and egress and to prevent oxidation of the refractory metal surfaces. The resulting membrane showed greater hydrogen transport than with palladium or its alloys, was strong, produced 100% pure hydrogen, and had a high tolerance to pinhole defects in the coat. Although the coat was not continuous, selectivity remained 100% because the nonporous substrate blocked non-hydrogen gas transport that penetrated defects in the coat.

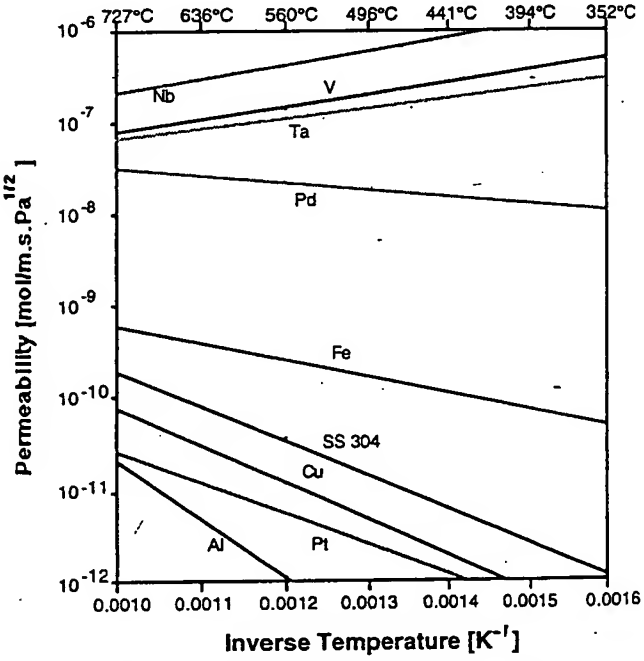

Figure 1. Hydrogen permeabilities of selected metals.

Makrides et al.'s membranes achieved limited application though because the coating process, palladium vapor deposition at high vacuum, was expensive and deficient. Vapor deposition does not coat inside tubes, the preferred extractor configuration, and generally retains significant surface transport resistance. Hydrogen transport, while higher than with palladium, was one-tenth that predicted from the data in Figure 1. Makrides et al.'s vapor-coated membranes found use only in the nuclear industry where the high cost is offset

* Author to whom correspondence is addressed. Phone: 810-547-7942. home page http://www.tcimet.net/reb/buxt.htm.

0888-5885/96/2635-0530$12.00/0

by the membranes' high flux and durability. A palladium-coated alloy membrane worked for over 10 000 h continuously, removing hydrogen from metal-cooled nuclear reactor fluids,[9] and palladium-coated zirconium has been tested successfully for removing embrittling deuterium from CANDU reactor bundles.[14]

More recently, Hsu and Buxbaum patented a lower-cost electroless deposition process for applying a uniform palladium coat to refractory metals, even inside tubes.[15] Amano et al.[19] demonstrated membranes of a nonembrittling vanadium alloy which extends the range of coated-membrane operation, in theory, down to room temperature. Also, flux measurements with coated tantalum, niobium, and zirconium disks have generally corroborated the predictions in Figure 1 and corroborated the predicted 100% hydrogen selectivity.[10,16] The permeance of a 0.25 mm wall niobium tube at 420 °C was found to be 0.0007 mol/m^2 s Pa$^{1/2}$, much higher than that for a Ube polymer membrane operating at 100 °C and these pressure drops.[16] However, the predicted cost was \$500/ft^2, more than double that for polymeric membranes.[31]

Background to Hydrogen Transport in Metals

Hydrogen transport through metals has been studied extensively.[11,13,17,18] Since hydrogen molecules dissociate into atoms to diffuse through metals, transport is calculated from the atomic flux. Fick's first law describes the flux of hydrogen atoms through a homogeneous phase as:

$$N_H = -D_M(\Delta C_H/\delta_M) \quad (1)$$

where N_H is the atomic flux, D_M is diffusivity, ΔC_H is the change in hydrogen atom concentration across the membrane, and δ_M is the membrane thickness. C_H is related to the partial pressure of hydrogen in equilibrium with the metal, correlated for example by

$$C_H = K_S(P^{1/2}) \quad (2)$$

where K_S is the Sieverts constant and P is the partial pressure of hydrogen in equilibrium with the metal. The power of $^1/_2$ comes from the dissociation of hydrogen molecules into twice as many atoms at low concentration.

We now calculate the flux of hydrogen molecules, N, in terms of pressure using eq 1 and 2. Since the flux of molecules is half the flux of atoms:

$$N = (D_M K_S/2\delta_M)\Delta P^{1/2}$$
$$= \mathscr{P}_M \Delta P^{1/2}/\delta_M \quad (3)$$

The term $\mathscr{P}_M$ above is called the metal permeability,

$$\mathscr{P}_M = D_M K_S/2 \quad (4)$$

a pressure-independent constant for a given metal at low hydrogen contents. Two derived quantities, the "permeance" and the "total resistance to transport", are respectively the flux divided by the pressure driving force and the inverse of this number. These numbers are related to the average permeability, $\mathscr{P}$.

$$\text{permeance} \equiv N/\Delta P^{1/2} = \mathscr{P}/\delta \quad (5)$$

$$R_{Tot} \equiv \Delta P^{1/2}/N = \delta/\mathscr{P} \quad (6)$$

In a multilayer membrane the total transport resistance of a membrane, R_{Tot}, is the sum of the resistance in each layer ($\sum \delta_M/\mathscr{P}_M$) plus the effective resistance caused by gas-phase diffusion.[6]

Permeabilities of the refractory metals vanadium, tantalum, zirconium, and niobium are so large that until recently they were inferred only from diffusivity and low concentration solubility coefficients via eq 4. These values are shown in Figure 1 along with experimental values for several nonrefractory metals. Recent measurements have confirmed the prediction that these metals are significantly more permeable than palladium.[10,16] Figure 1 shows $\mathscr{P}_M$ for some metals increasing with decreasing temperature. This temperature dependence occurs when hydrogen absorption is more exothermic than the activation energy for diffusion is endothermic, e.g., with palladium-coated zirconium.[10]

In polymer and porous ceramic membranes, flux is proportional to ΔP, not to $\Delta P^{1/2}$ as with metal membranes. Because of this, metal membranes are more attractive at low hydrogen pressures. This is seen by approximating for $\Delta P^{1/2}$ from the derivative with respect to P,

$$P^{1/2} \approx \Delta P/2\bar{P}^{1/2}$$

where $\bar{P}$ is the average hydrogen partial pressure. Combining this with eq 3 for flux through a metal membrane

$$N \approx (\mathscr{P}_M/2\delta_M\bar{P}^{1/2})\Delta P$$

flux per pressure drop decreases with increasing hydrogen pressure. In a polymer or ceramic this permeance is measured in barrers and is fairly pressure independent.

High hydrogen concentrations tend to decrease a metal's diffusivity but increase its Sieverts constant.[17,20] The hydrogen diffusivity decreases because the nearest-neighbor sites for hydrogen atom jumps become filled.[20] Because hydrogen concentration increases with decreasing temperature, this effect tends to flatten the temperature dependence of the hydrogen permeability. The Sieverts constant rises with increasing concentration because the hydrogen atoms attract. The net effect is that fluxes are effected little but often vary from the pressure to the $^1/_2$ expectation. Palladium-coated tantalum and niobium disks show permeabilities similar to Figure 1, but the temperature effect is flattened.[16] This paper will discuss pressure effects.

Gas-phase transport resistance, surface resistance (dissociation/ recombination), and interface effects can also affect transport,[13,21,22,27] and several modifications of eq 3 include these resistances.[7,21,22] With proper coating, though, interface resistance can be removed almost completely.[13,23] Similarly, dissociation on palladium presents little transport resistance even at temperatures as low as 325 °C[10] unless fouling is present. Palladium is fairly immune to surface poisoning,[28-30] but since these membranes are so permeable, they may foul with impurity concentrations that would go unnoticed with homogeneous palladium or alloys. Also, because the membranes are extremely permeable and are 100% selective, gas-phase mass transport resistance can appear at flows and geometries which would be inconceivable with other membranes.

The experimental setup is shown in Figures 2 and 3. We use tubular membranes rather than the flat disks used previously[16] because tubes allow a thinner wall for

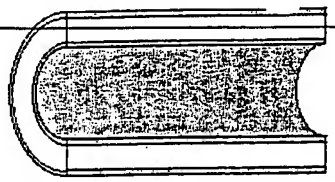

Figure 2. Cutaway diagram of a tubular membrane.

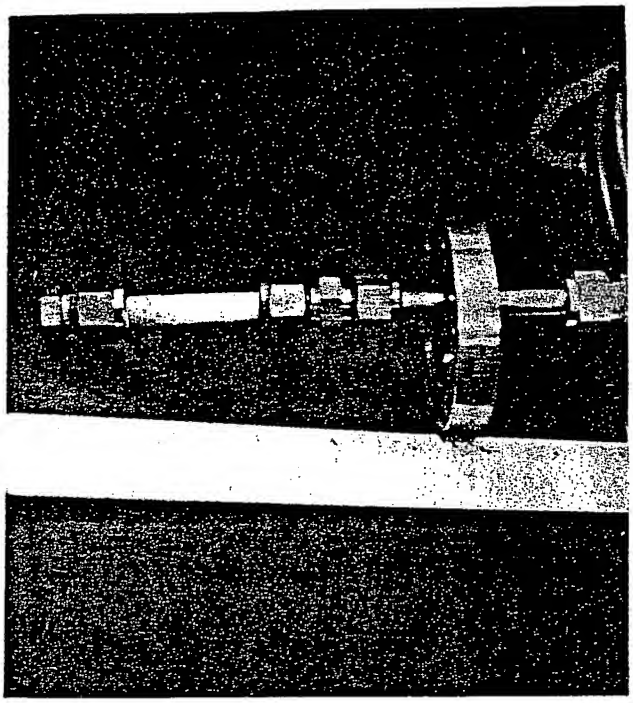

Figure 3. Phototgraph of a membrane in a Swagelok holder.

a given pressure differential, and thus allow higher hydrogen fluxes. Also, tubular membranes are easily fabricated into large-scale hydrogen extractors using a shell-and-tube heat-exchanger design.

Most of the experiments presented here use tantalum because tantalum showed less hydrogen embrittlement. Niobium is somewhat cheaper and more permeable to hydrogen than tantalum but is more readily embrittled.[16] Several alloys have shown higher hydrogen permeability than these elements and avoid hydrogen embrittlement entirely, but none are as readily available in tube form.

Preparing, Coating, and Evaluating Tubular Membranes

We started with commercial-grade tantalum heat-exchanger tubes $^3/_8$ in. in diameter in four wall thicknesses (0.054, 0.037, 0.027, and 0.007 cm) and with a niobium tube ($^3/_8$-in.-diameter, 0.034-cm wall). Tube lengths were between 4 and 41 in. The surfaces of these tubes arrive from the manufacturer coated with a layer of oxide and often with a layer of oil. Both of these interfere with the coating process and must be removed in order to make an acceptable membrane. Gross oxide and oil was removed by abrasion and detergent. We then electropolished, hydrided, and applied our electroless palladium coat as described previously.[15] For several of the coated tubes, we used hydrazine as the reducing agent instead of hypophosphate. Hypophosphate was found to deposit palladium–5% phosphorus,[24,25] and we hoped to find superior performance with a purer palladium coat produced by reducing with hydrazine.

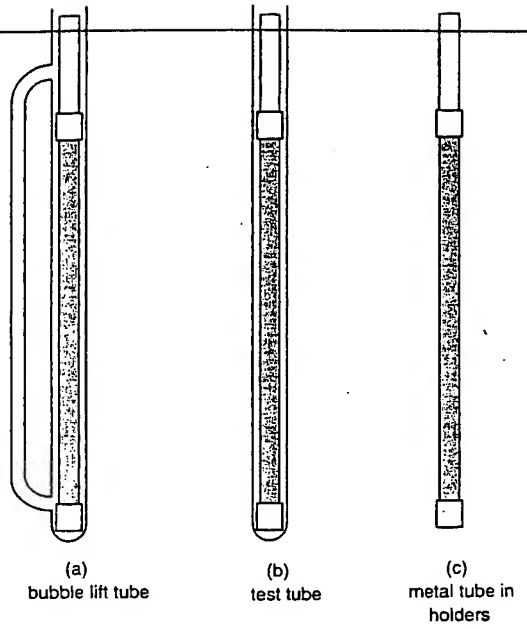

Figure 4. Electroless coating setups.

With several tubes the solution was mixed continuously during plating by performing the plating in a test tube with a side arm (Figure 4a). Here, gas that evolves during coating causes an upward flow of solution, and the side arm allows a return flow once the bubbles leave (gas-lift circulation). We thought such circulation might improve the coat. The rest of the membranes were coated in large test tubes (Figure 4b) and stirred only occasionally. In all, we coated more than 60 tantalum tubes and 20 niobium tubes.

Several membranes were annealed at high pressure (HIPing) by sealing the apparatus exits and pressurizing with 100 psi of argon. Membranes were heated to 500–525 °C and kept this way for several hours or days to see whether higher hydrogen fluxes resulted from an improved bond between the palladium and the substrate. Sawatzki and Ledoux[14] found that annealing for 4 h at 700 °C improved hydrogen removal from a palladium-coated zirconium tube, presumably because of increased bonding.

Permeability and Durability Measurement

The permeabilities of the palladium-coated metal membranes were studied using the apparatus shown in Figures 5 and 6. The membranes were reliably sealed into the apparatus via swageloks (Figure 5). We use graphite ferrules to allow the membrane to swell without stress embrittlement or leaks.

Impure hydrogen–gas, or a mixture of hydrogen and argon, enters the apparatus as indicated by the arrows in Figures 5 and 6. The gases travel up the outside of the module while being heated to operation temperature, they then flow down the inside of the apparatus and contact the membrane. Much of the hydrogen permeates the membrane, and the rest exits along with the argon or impurities. We measure the flow rate of hydrogen through the membrane and the gas pressures at the inlet and exits (Figure 6). From this and the membrane area, we calculate the effective permeance of the membrane via eq 5. The total membrane resistance is then the inverse of the permeance and equals the sum of mass-transfer resistances in the palladium, in the tantalum, in the interface (if any), and in the

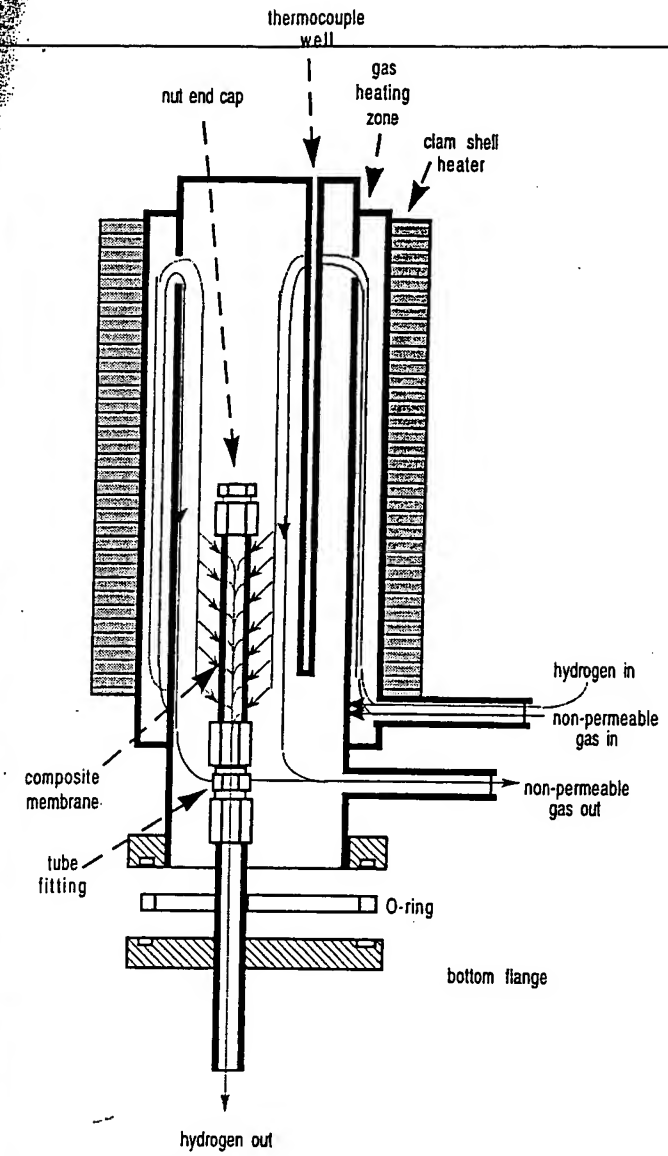

Figure 5. Membrane permeation apparatus.

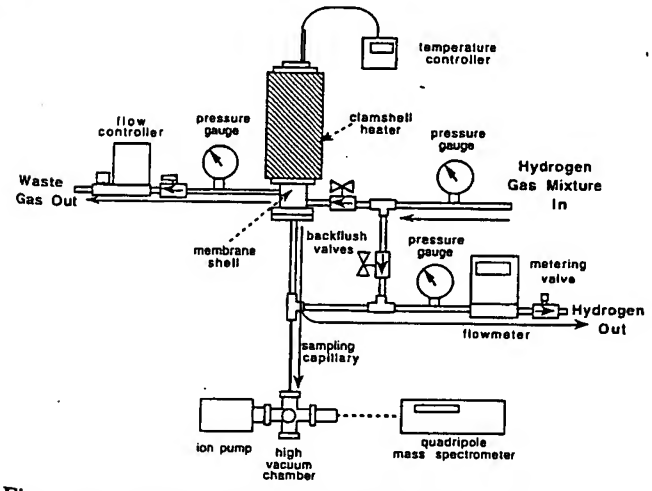

Figure 6. Membrane test apparatus showing flows.

flowing gas stream. The effective membrane permeability is calculated from the permeance and thickness via eq 5.

Durability tests involved measuring the permeation flux continuously for several weeks. During durability testing membranes were given weekly backflushes with hydrogen to drive off coke and other contamination that may have agglomerated on the upstream membrane surface. Backflushing was done by reversing the hydrogen flux through the membrane.

As with our earlier experiments,[10] we regularly check for leaks by analyzing the output hydrogen purity, here using an on-line mass spectrometer (Figure 6). Any sign of argon in the output is evidence of a leak, and we shut down. Except when testing for leaks, the membrane is run with Matheson 99.8% pure hydrogen as a feed and 98% hydrogen (approximately) as a purge. This purity was chosen to minimize gas-phase mass-transfer resistance, while getting an industrially-significant measure of the permeance. Gas-phase mass-transfer resistance can be very large with these membranes because of the very high hydrogen fluxes.

Electron Microscopy, X-ray, and Auger Spectroscopy

Electron microscopic and X-ray examination of the coat was used extensively because it gave an excellent image of coat thickness and uniformity at the magnifications of interest, about 5000×. A combination of Auger and X-ray spectroscopy was used to determine elemental compositions of the coat and of the interface. Auger spectroscopy was used to determine that there were no foreign elements at the surfaces or interfaces, but because of the small spot size, it is easily confused by oxygen or water that adheres to the sample surface during mounting. X-ray spectroscopy scans a much larger volume, making it more accurate for studying coat composition, but it is insensitive to all but the grossest interdiffusion effects, and it is blind to oxygen, nitrogen, and carbon contaminants.

Results: Solution Coating and Stirring

We coated several 18 in. long membranes in the simple test tubes (Figure 4b), stirring occasionally by hand. We coated several others (including the largest membrane, 41 in. long) using gas-lift solution circulation (Figure 4a). In either apparatus a 1−3 μm palladium coat requires from 4 to 12 h. We could detect no improvement in coat quality from gas-lift circulation, and since this technique is cumbersome, we recommend using simple test tubes.

The coat formed more readily using hydrazine as the reducing agent instead of hypophosphate. The composition of membranes using Auger spectrometry showed that the Pd coats produced using hypophosphate contained 5% phosphorus impurity and showed some metallic interdiffusion at 420 °C. The newer hydrazine-based coats showed no detectable impurities and no clear sign of interdiffusion. Figure 7 suggests that the transport resistance is somewhat lower with hydrazine as well.

After long periods of operation, especially at high temperatures, the palladium surface tended to turn darker than at first. Auger, electron microscope and X-ray analysis comparing membranes before and after operation showed no clear sign of interdiffusion but showed a surface morphological change. Apparently, we are making "palladium black", the palladium equivalent of platinum-black catalyst. This increased surface roughness may explain the observation that flux increases during the first few hours of operation and eventually decreases (see below). Figure 3 shows a membrane after 31 days of operation at 420 °C; surface darkening is seen at the tube end near the ferrule. We

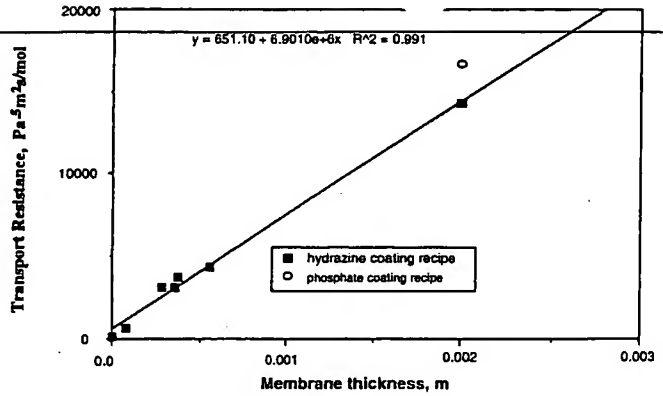

Figure 7. Transport resistance in palladium-coated Ta membranes at 420 °C; two coating recipes.

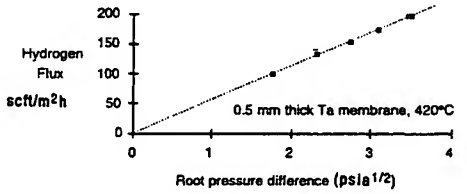

Figure 8. Hydrogen flux vs. root pressure difference.

suspect that surface darkening is caused by defect migration from below. These defects may have been caused by expansion of the palladium or refractory metal during hydrogen absorption.[27] We could test this hypothesis by replacing the pure metal palladium and substrates with less defect-prone alloys or by charging the substrate with different amounts of hydrogen before coating.

When observed with Auger spectroscopy, all coats showed significant surface carbon and oxygen. This contamination is probably due to exposure to the atmosphere during sample mounting and is probably not representative of the permeation environment.

Membrane Permeability

Figure 7 plots the effective resistance of several membranes as a function of refractory metal thickness. As expected from eq 6, resistance increases in proportion to membrane thickness, but Figure 7 also suggests that transport resistance is somewhat higher with the older phosphate recipe than with the newer recipe. A positive intercept is expected in this plot, representing transport resistance through the palladium coat, surfaces, and interfaces. The correlation coefficient for the linear fit is 0.991, including only membranes coated by the newer recipe.

The slope of the line in Figure 7 should be inversely proportional to the tantalum permeability for any fixed surface or palladium transport resistance (eq 3), i.e., $\mathscr{P}_M = 1/(\Delta R_M/\Delta\delta_M)$. Surface and fixed palladium-layer resistances affect only the intercept of this line, assuming only that they remain constant throughout. Thus at 420 °C, the average permeability of tantalum equals $1/6.901 \times 10^6$ or 1.45×10^{-7} mol/m s $Pa^{1/2}$. This value is in close agreement with Figure 1. Our previously reported value for the permeability of tantalum was 30% lower,[16] but this value was not corrected for surface resistance.

Figure 8 shows the hydrogen flux with a thick-walled palladium-tantalum membrane as a function of pressure differential at 420 °C. The upstream pressures ranged from 1 to 3 atm, and downstream pressures ranged from

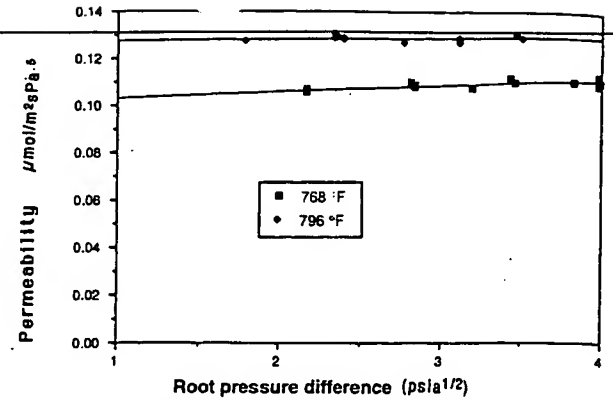

Figure 9. Tantalum membrane permeability vs temperature and pressure.

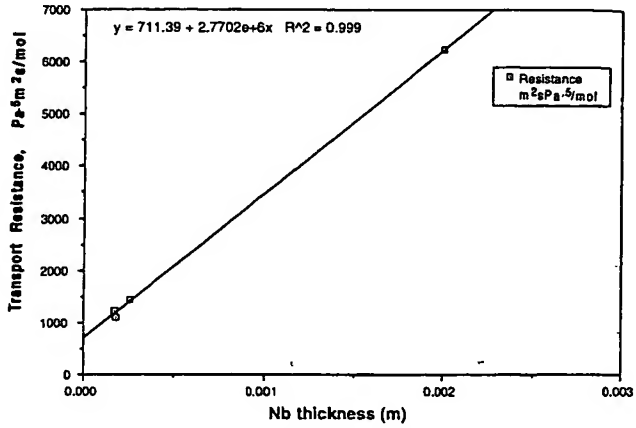

Figure 10. Transport resistance in Nb-based membranes vs membrane thickness.

near vacuum to about 1.5 atm. For all driving pressures studied, flux is nearly proportional to pressure difference to the $^1/_2$ power, agreeing with eq 3. The average effective permeability here is 1.2×10^{-7}, somewhat lower than the above because of resistance in the palladium coat and at the palladium surfaces. Still this is 10 times higher than the permeability of palladium alloys at this temperature, about 1.2×10^{-8} mol/m s $Pa^{1/2}$. Even with thin-walled palladium membranes, the flux is about $^1/_5$ the values in Figure 8.

Figure 9 shows the effective permeability of a palladium-coated tantalum membrane as a function of pressure at two temperatures. At both temperatures, it appears that permeability is fairly independent of hydrogen pressure. This is not to say that D_M and K_S are pressure-independent, only that the product of D_M and K_S varies only weakly with H concentration at these temperatures. The permeability is seen to increase with temperature, contrary to the prediction in Figure 1 but in agreement with our previous findings.[19]

Niobium Membranes

Niobium heat-exchanger tubes up to 18 in. long were coated with palladium using the same techniques used for the tantalum tubes above. The transport resistance with these membranes is shown in Figure 10. As with tantalum, transport resistance in Nb-based membranes increases linearly with thickness in accordance with eq 5. The intercept resistance in Figure 10 is higher than with tantalum (Figure 7). This higher intercept with niobium may reflect surface resistances or may represent a poorer coating technique. The average permeability in niobium, determined from the slope of the line

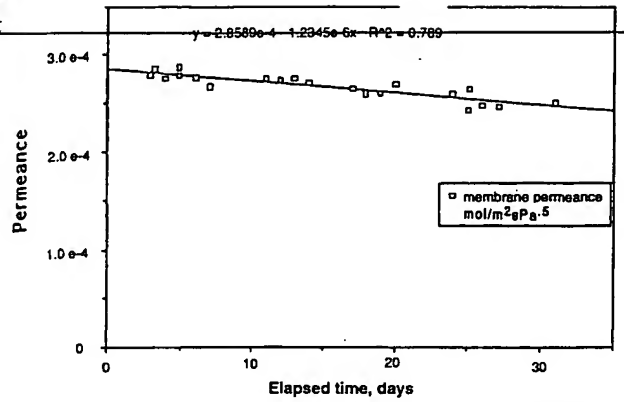

Figure 11. Permeance of a palladium-coated tantalum membrane run for 31 days at 420 °C with weekly backflushes.

as above, is 3.6×10^{-7} mol/m s $Pa^{1/2}$. This is 2-1/2 times the permeability of tantalum and is almost identical to the value measured using thick niobium disks.[16] This value, however, is about half the prediction in Figure 1.

The maximum permeance of our Nb-based membranes was 0.0011 mol/m^2 s $Pa^{1/2}$, 75% that of the thinnest-wall tantalum-based membranes. This lower permeance could be improved if thinner walled niobium were used; the thinnest-wall niobium membranes were 0.15 mm thick, twice the thinnest-wall tantalum membranes.

Membrane Durability

Commercial membranes should last a few months to a few years in service with only minimal loss of flux. To test our membrane's durability, we measured the flux in several membranes for periods up to 31 days.

A tantalum-based membrane that was run for 31 days at 420 °C is shown in Figure 3. It looks like new except for a slight darkening near the upper ferrule as discussed above. Figure 11 shows that the permeance of this membrane decreases with time, decreasing about 15% over 31 days of operation. The decrease is approximately linear with time, varying only slightly on a daily basis, presumably due to variations in gauge readings, atmospheric pressure, and the effect of weekly backflushes. Weekly backflushing with hydrogen is found to increase the flux by a few percent. Membranes coated using the older phosphate recipe deteriorated somewhat faster, possibly because of the difficulty in getting a good coat.

Hydrogen embrittlement was a serious problem with tantalum and niobium membranes. The minimum temperature for tantalum membranes was 350 °C, dictated by the need to avoid embrittlement cracking. The minimum temperature for niobium membranes was 420 °C for the same reason. Cracking is also affected by hydrogen pressure, metal annealing, and thickness and by the tightness of the ferrules.

Discussion

The flux with these membranes is about that predicted from theory and earlier experiments but increases with temperature, contrary to our simple expectations for Ta and Nb. Two effects may cause this behavior. First, the palladium coat adds a resistance and this resistance decreases with increasing temperature. Further, as temperatures increase, the hydrogen content decreases and this increases diffusion rates by increasing the number of vacant sites next to the hydrogen atoms.[20] These two effects could cause the rise in effective membrane permeability for the pressures and Pd thicknesses studied.

The thinnest membranes, made from 0.07 mm wall tantalum tubes, show transport resistance of 700 m^2 s $Pa^{1/2}$/mol (permeances of 0.00147 mol/m^2 s $Pa^{1/2}$). Fluxes with such membranes are higher than those with any other nonporous membrane that we know of and continue to increase with decreasing tantalum thickness. This suggests that the major transport resistance is in the substrate, at least for the membrane thicknesses studied.

The flux is higher than with the commercial polymeric membranes, but the cost seems higher as well, currently this is about \$500/ft^2 as compared with \$200/ft^2 for polymers.[31] Thus, flux and price are in the range for economical application. Scaleup and fabrication do not seem to be a serious problem since the coating methods are simple. The membranes are attached by standard swageloks. The 15% decrease in flux for 31 days is a serious concern, though, since the root causes are not clear at this stage.

Membrane life will have to be extended to 1 year or so before they are ready for commercial use. If transport resistance adds at the steady rate of 15%/month, as appears from Figure 11, the membrane flux would fall below 50% in 6–7 months. We have tried several "cures" at this stage, and none has worked completely. Presuming that the cause was small amounts of impurity concentrating at the metal surface (fouling), we tried backflushes as described above. This helped but did not completely erase the deterioration, possibly a longer backflush is needed. Alternatively, if the observed morphological changes caused deterioration, maybe a low-swelling alloy would deteriorate slower than the pure metals used here. Alternatively, deterioration may be due to interdiffusion of the palladium and substrate as suggested by Edlund.[26] This is the "best result" since interdiffusion would tend to slow on its own as the interdiffusion layer grew. Thus, the membrane tested in Figure 11 might be expected to operate for years before the flux dropped 50%. Edlund et al.[26] found evidence for intermetallic interdiffusion at 700 °C, but the flux decrease in Figure 11 looks too steady for this explanation. Deterioration shows no slowing as the interdiffusion zone increases, but our experiments were of short duration. Longer term experiments will show whether interdiffusion is the cause.

In a preliminary experiment we were able to reverse this deterioration completely by replacing the palladium surface with fresh palladium. More experiments are being conducted in this area.

Sample Design, Hydrogen Extraction from Hydrotreater Off-Gas

Hydrogen is used in petrochemical plants for hydrodesulfurization and for methanol and ammonia synthesis. Additional hydrogen has a value in such plants because it reduces plant energy costs and allows more flexible operation, e.g., it allows production of a "reformulated" gasoline that maintains current octane levels but has fewer aromatics (aromatics are carcinogenic, polluting components of gasoline). A common route to reformulated gasoline is to reduce the flow and temperatures in reformer units while increasing the flow and temperature in Catcracker fluidized-bed reactors.

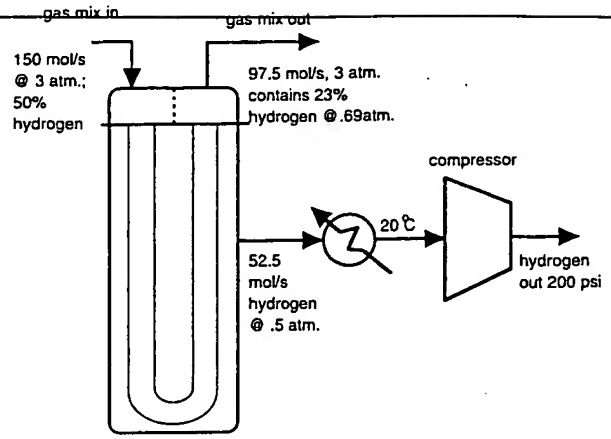

Figure 12. Setup for hydrogen removal from hydrotreater off-gas.

This change reduces the amount of reformer hydrogen available for hydrodesulfurization and resid upgrading, so this route requires a source of additional hydrogen. Depending on the plant, pure hydrogen has a chemical value about \$2.00/kg mol (\$0.002/g mol) above its fuel value.[26,27]

We will consider a modestly large stream of hydrotreater off-gas: 10 000 000 scf/day at 3 atm, containing 50% hydrogen mixed with methane, ethane, water, and CO_2. Refineries produce and burn such streams as "fuel gas" because the low-pressure hydrogen is too expensive to recover. We will recover 70% of this hydrogen using a metal membrane-based extractor in the shape of a shell and tube heat exchanger (Figure 12). The gas mixture flows through the tubes, while the hydrogen is recovered from the shell. The double-pass, vertical-standing design minimizes problems of metal expansion and membrane support. In SI units, the flow is 150 mol/s, with hydrogen making up 75 mol/s; if 70% is recovered, this is 52.5 mol/s (3.5 MMscft/day).

For a benchmark design, consider 420 °C operation, using 1 cm diameter tubes of our best current palladium-covered tantalum. These tubes have a permeance of 0.001 47 mol/m^2 s Pa$^{1/2}$, are strong enough for the pressures and temperatures needed, and, because of their large diameter, add minimal gas-phase pressure drop. Still, the hydrogen pressure in the shell must be lower than the minimum hydrogen partial pressure in the tubes since this pressure difference drives the extraction. The minimum hydrogen pressure in the tubes is:

$$H_2 \text{ partial pressure} = \frac{(3 \text{ atm}) \times (22.5 \text{ mol/s unrecovered } H_2)}{97.5 \text{ exiting mol/s}} = 0.69 \text{ atm} \quad (7)$$

For design purposes, pick a hydrogen shell pressure of half this, 0.35 atm. (It is generally recognized that polymer membranes are not economical at such low-pressure gradients.)

The membrane surface area is calculated from the permeance, 0.001 47 mol/m^2 s Pa$^{1/2}$:

$$\text{flux}, N = \frac{52.5 \text{ mol/s}}{\text{area}} = P_{up}^{1/2} - P_{dn}^{1/2} \text{ (permeance)} \quad (8)$$

where P_{up} is the average hydrogen partial pressure in the tube, P_{dn} is the hydrogen pressure in the shell, and 52.5 mol/s is the design load. P_{up} varies between 1.5 atm at the tube inlet and 0.69 atm at the tube outlet, but for eq 8, let us use the geometric average 1.0 atm, or 100 000 Pa in SI units. The downstream hydrogen pressure is 0.35 atm, or 35 000 Pa. The flux is thus

$$N = (316.2 - 187.1 \text{ Pa}^{1/2})(0.00147) = 0.190 \text{ mol/m}^2 \text{ s}$$

From eq 7, the membrane area is

$$A = (52.5 \text{ mol/s})/(0.190 \text{ mol/m}^2 \text{ s}) = 276 \text{ m}^2$$

For an extractor of this area, the shell could be 5.5 m long, containing doubled tubes 10 m long. Since each 1 cm diameter × 10 m tube has a surface area of 0.314 m^2, the extractor will use 880 tubes for a total tube length of 8800 m, or 27 500 ft. The shell diameter for this number of tubes would be about 1 m.

A series of intercooled compressors is now chosen to bring the hydrogen to 200 psi for general plant use. Steam sparging is a cheaper alternative for the first stage of hydrogen compression, but it contaminates the hydrogen with water vapor.

Economics of Hydrogen Recovery with This Extractor

The adiabatic pumping cost is estimated as the isothermal compression work at 400 K, an average gas temperature assuming inefficient intercooling.

$$W = RT \ln(P_f/P_i) = 8.314 \times 400 \times 3.660 = 12 \text{ kJ/mol} \quad (9)$$

At 7.5¢/kwh this operating cost is 0.025¢/mol.

The total equipment cost is now calculated from the cost of tubes, shell, pumps, etc. Large runs of uncoated tantalum tubes are priced at about \$15/ft. Coating 1 μm of Pd on each side is estimated to add an additional \$5/ft, and thus the membranes cost about \$20/ft, or 0.55 M\$ total. Added to this are the purchase cost of the shell, fabrication, control, and heat exchanger, an additional \$200 000. The projected capital cost excluding pumps is thus 0.75 M\$, which is increased to 1.25 M\$ including the price of rotary vane pumps.

This capital cost must be compared to the value of the recovered hydrogen minus operating costs. Assuming the hydrogen is worth 0.2¢/mol more than its fuel value and operating costs are 0.025¢/mol as calculated above, operating profit is

$$(52.5 \text{ [mol/s]}) \times (0.002 - 0.000\,25 \text{ [\$/mol]}) \times (3.15 \times 10^7 \text{ [s/yr]}) = 2.9 \text{ M\$/yr}$$

Given the capital cost of 1.25 M\$, the payback period is less than 5 months, which is excellent. The calculations can be redone using our current membrane cost, \$45/ft, and the payback period is found to be less than 8 months, which is still excellent. Optimization should result in improved economics.

Acknowledgment

We gratefully acknowledge financial support from the Department of Energy under Phase 1 and 2 SBIR grants, No. DE-FG02-93ER81625.

Literature Cited

(1) Armor, J. N. Catalysis with Permselective Inorganic Membranes. *Appl. Catal.* **1992**, *49*, 1–25. Also: Armor, J. N. *CHEMTECH* **1992**, *22*, 557–563.

(2) Phillpott, J.; Coupland, D. R. Metal ... mbranes for Hydrogen Diffusion and Catalysis. *Hydrogen Effects in Catalysis*, Paal, Z., Menon, P. G., Eds.; Marcel Dekker: New York, 1988; pp 679–694.

(3) Tsotis, T. T.; Champaginie, A. M.; Vasileiadis, S. P.; Zaika, Z. D.; Minet, R. G. The Enhancement of Reaction Yield through High Temperature Membrane Reactors. *Sep. Sci. Technol.* **1993**, *28*, 397–422.

(4) Makrides, A. C.; Wright, M. A.; Jewett, D. N. Separation of Hydrogen by Permeation. U.S. Patent 3,350,846, Nov 7, 1967.

(5) Hsu, C.; Buxbaum, R. E. *J. Electrochem. Soc.* **1985**, *132*, 2419.

(6) Hsu, C.; Buxbaum, R. E. *J. Nucl. Mater.* **1986**, *141–143*, 238.

(7) Buxbaum, R. E. *Sep. Sci. Technol.* **1983**, *18*, 1251.

(8) Perng, T. P.; Altstetter, C. J. *Metall. Trans.* **1986**, *17A*, 2086–2090.

(9) Hill, E. F. Feasibility Study: Removal of Tritium from Sodium During the MDEC Process by Oxidative Diffusion. Argonne West, DOE N707T1830035, 1982.

(10) Buxbaum, R. E.; Hsu, P. C. *J. Nucl. Mater.* **1992**, *189*, 183–192.

(11) Steward, S. A. Review of Hydrogen Isotope Permeability through Materials. Lawrence Livermore National Laboratory Report, UCRL-53441, 1983.

(12) Buxbaum, R. E. Composite Metal Membranes for Hydrogen Extraction. U.S. Patent 5,108,724, Dec 15, 1991.

(13) Pick, M. A. *Proceedings NATO Institute on Metal Hydrides*; Bambakidis, G., Ed.; Plenum Press: New York, 1981; pp 329–343. Review works by: Pick, M. A.; Davenport, J. W.; Strongin, M.; Dienes, G. J. *Phys. Rev. Lett.* **1979**, *43*, 286–289. Pick, M. A.; Greene, M. G.; Strongen, M. *J. Less-Common Met.* **1980**, *73*, 89.

(14) Sawatzki, A.; Ledoux, G. A. The Use of Palladium to Remove Hydrogen from Zirconium. Presented at the 2nd International Congress on Hydrogen in Metals, Paris, France, 1977.

(15) Buxbaum, R. E.; Hsu, P. C. Method for Plating Palladium. U.S. Patent 5,149,420, issued Sep 22, 1992.

(16) Buxbaum, R. E.; Marker, T. L. Hydrogen Transport in Nonporous membranes of Palladium-coated Niobium, Tantalum, and Vanadium. *J. Membr. Sci.* **1993**, *89*, 29–38.

(17) Kleiner, J. E.; Sevilla, E. H.; Cotts, R. M. Diffusion of Hydrogen in a′-VH_x. *Phys. Rev. B* **1986**, *33*, 6662.

(18) Hemplelmann, R. Diffusion of Hydrogen in Metals. *J. Less-Common Met.* **1984**, *101*, 69–97. All of this special volume concerns hydrogen in metals.

(19) Amano, M.; Komaski, M.; Nishimura, C. Hydrogen Permeation Characteristics of Palladium Plated V–Ni Alloy Membranes. *J. Less-Common Met.* **1991**, *172–174*, 727–731.

(20) Peterson, D. T.; Jensen, C. L. Diffusion of Hydrogen in Niobium–Tantalum Alloys at 296 K. *Metall. Trans. A* **1980**, *11A*, 627–631.

(21) Zarchy, A. S. L. ...ations on Hydrogenic Gas Transport at Ultra-Low Pressures. Ph.D. Thesis, Princeton University, 1978, University Microfilms, pp 10–19.

(22) Fukada, S.; Nakahara, T.; Mitsuishi, N. *J. Nucl. Mater.* **1990**, *171*, 399–407.

(23) Kumar, V.; Bennemann, K. H. Electronic Structure of Transition Metal–Transition Metal Interfaces: Pd on Nb(110). *Phys. Rev. B* **1983**, *28*, 3138–3149.

(24) Govind, R.; Atnoor, S. Development of a Composite Palladium Membrane for Selective Hydrogen Separation at High Temperature. *Ind. Eng. Chem. Res.* 1991, *30*, 157–158. See also: Itoh, N.; Govind, R. Development of a Novel Oxidative Palladium Membrane Reactor. *AIChE Symp. Ser.* **1989**, *268*, 10–17. Ilias, S.; Govind, R. Development of High Temperature Membranes for Membrane Reactors, an Overview. *AIChE Symp. Ser.* **1989**, *268*, 18–25.

(25) Paunovic, M. *Proc. Symp. Electroless Deposition Met. Alloys* **1988**, 252–258.

(26) Edlund, D. Metal Membranes for High Temperature Gas Separations. *Proceedings of the 1990 Membrane Conference*, Business Communications, Norwalk, CT, 1991; p 77.

(27) Shu, J.; Grandjean, B. P. A.; VanNeste, A.; Kaliaguine, S. Catalytic Palladium-Based Membrane Reactors: A Review. *Can J. Chem. Eng.* **1991**, *69*, 1036–1060.

(28) Uemiya, S.; Kude, Y.; Sugino, K.; Sato, N.; Matuda, T.; Kikuchi, E. A Palladium–Porous glass Composite Membrane for Hydrogen Separation. *Chem. Lett.* **1988**, *10*, 1687–1690.

(29) Collins, J. P.; Way, J. D. Preparation and Characterization of a Composite Palladium–Ceramic Membrane. *Ind. Eng. Chem. Res.* **1993**, *32*, 3006–3013.

(30) Ali, J. K.; Newson, E. J.; Rippin, D. W. T. Exceeding Equilibrium Conversion with a Catalytic Membrane Reactor for the Dehydrogenation of Methylcyclohexane. *Chem. Eng. Sci.* **1994**, *49*, 2129–2134.

(31) Johnson, H. E.; Schulman, B. L. Assessment of the Potential for Reinery Applications of Inorganic Membrane Technology—an Identification and Screening Analysis. U.S. DOE Report, DOE/FE-60680-H3, May 1993.

Received for review August 24, 1995
Accepted October 31, 1995[⊗]

IE950105O

[⊗] Abstract published in *Advance ACS Abstracts,* January 1, 1996.